frontiers | Frontiers in Immunology

TYPE Original Research
PUBLISHED 14 August 2025
DOI 10.3389/fimmu.2025.1583493

OPEN ACCESS

EDITED BY
Kosuke Nishi,
Ehime University, Japan

REVIEWED BY
Amit Kumar Singh,
National Institute on Aging, United States
Xingwu Zhou,
University of Michigan, United States

*CORRESPONDENCE
Mourad Aribi
mourad.aribi@univ-tlemcen.dz;
m_aribi@yahoo.fr;
m_aribi@outlook.fr
Abdelouahab Bellou
abellou402@gmail.com

†These authors share senior authorship

RECEIVED 26 February 2025
ACCEPTED 16 June 2025
PUBLISHED 14 August 2025

CITATION
Meterfi FS, Zoudji S, Bendjeffel NE, Messali R, Boudjelal F, El Mezouar C, Brikci Nigassa N, Mekkaoui Z, Brikhou S, Mennechet FJ, Touil-Boukoffa C, Li X, Bellou A and Aribi M (2025) Passive physical barrier modulates UVB-induced METosis-related MPO expression and activity, 25-hydroxyvitamin D3-1alpha-hydroxylase, and the shift of tissue-resident macrophages toward M1-associated iNOS. *Front. Immunol.* 16:1583493. doi: 10.3389/fimmu.2025.1583493

Passive physical barrier modulates UVB-induced METosis-related MPO expression and activity, 25-hydroxyvitamin D3-1alpha-hydroxylase, and the shift of tissue-resident macrophages toward M1-associated iNOS

Farah Sara Meterfi[1], Souad Zoudji[1], Nour Elhouda Bendjeffel[1], Rabia Messali[1], Fadila Boudjelal[1], Chahrazed El Mezouar[1,2], Nawal Brikci Nigassa[1,3], Zineb Mekkaoui[1], Slimane Brikhou[1], Franck JD Mennechet[4†], Chafia Touil-Boukoffa[1,5†], Xin Li[6,7†], Abdelouahab Bellou[1,7,8,9,10,11*] and Mourad Aribi[1,7,12*]

[1]Laboratory of Applied Molecular Biology and Immunology, University of Tlemcen, Tlemcen, Algeria, [2]Pediatrics Department, Mother and Child Specialized Hospital of Tlemcen, Tlemcen, Algeria, [3]Biochemistry Department, Tlemcen University Hospital Center, Tlemcen, Algeria, [4]Pathogenesis and Control of Chronic and Emerging Infections, The Institut National de la Santé et de la Recherche Médicale (INSERM) U1058, University of Montpellier, Etablissement Français du Sang, Antilles University, Montpellier, France, [5]Algerian Academy of Sciences and Technologies (AAST), El Madania, Algiers, Algeria, [6]Shenzhen Key Laboratory of Viral Oncology, The Clinical Innovation and Research Center (CIRC), Shenzhen Hospital, Southern Medical University, Shenzhen, China, [7]China-Algeria International Joint Laboratory on Emergency Medicine and Immunology, Guangdong Provincial, People's Hospital (Guangdong Academy of Medical Sciences), Southern Medical University, Guangzhou, China, [8]Institute of Sciences in Emergency Medicine, Department of Emergency Medicine, Guangdong Provincial People's Hospital (Guangdong Academy of Medical Sciences), Southern Medical University, Guangzhou, China, [9]Medical Research Institute, Guangdong Provincial People's Hospital (Guangdong Academy of Medical Sciences), Southern Medical University, Guangzhou, China, [10]Department of Emergency Medicine, Wayne State University School of Medicine, Detroit, MI, United States, [11]Global Network on Emergency Medicine, Brookline, MA, United States, [12]Biotechnology Research Center (CRBt), Constantine, Algeria

Background: This study investigated the role of UVB radiation and the influence of a simulated passive barrier on the enzymatic conversion of 25-hydroxyvitamin D3 (25(OH)D_3) by 1-alpha hydroxylase and its effects on the functional activity of tissue-resident macrophages.

Methods: Murine peritoneal tissue-resident macrophages (PRMφs) were exposed to three conditions: (1) Baseline (Control group), with no light exposure; (2) UVB+/RF- group, exposed to UVB rays without passive barrier simulation; (3) UVB+/RF+ group, UVB exposure with a thin layer of rat fur to mimic the passive barrier on the skin.

Results: UVB exposure did not significantly alter 25OHD_3 levels across groups but led to a marked downregulation of 1-alpha hydroxylase, particularly with the

10.3389/fimmu.2025.1583493

simulated barrier. UVB slightly enhanced phagocytosis and significantly increased nitric oxide (NO) and hydrogen peroxide (H_2O_2) production. Moreover, hypochlorous acid (HOCl) levels were significantly upregulated in the UVB-exposed PRMφ group, whereas they returned to baseline levels in the UVB+/RF + group. Furthermore, both MPO expression and activity were markedly upregulated after UVB exposure and downregulated in UVB+/RF+ group, suggesting that the overall effect of UVB on METosis-related MPO activity was substantially attenuated by the simulated barrier (for both comparisons, $p < 0.001$ by ANOVA test). Additionally, UVB exposure shifted PRMφs toward M1-phenotype, as evidenced by decreased ARG1 activity and increased iNOS activity and $M1_{(iNOS)}$-to-$M2_{(ARG1)}$ ratio. Additionally, UVB downregulated catalase (CAT) activity and intracellular glucose ($_{i}$GLU) levels, with a stronger effect in the barrier group. While UVB increased total cellular cholesterol content ($_{tcc}$CHOL), this effect was mitigated by the barrier. Finally, intracellular free calcium ion ($_{if}Ca^{2+}$) levels remained unaffected by UVB but showed a slight increase with the barrier.

Conclusions: UVB exposure enhances tissue-resident macrophage function in a preclinical rat model, increasing respiratory burst, phagocytosis, and M1-like polarization. The simulated barrier modulates these effects, notably by reducing MPO expression and METosis-related activity, which suggests a potential attenuation of excessive inflammation. These findings provide valuable insights relevant to human immune modulation and support further translational research. Future studies should investigate the role of circadian rhythms and other cell types in UVB- and vitamin D-mediated immune modulation.

KEYWORDS

25-hydroxyvitamin D3-1alpha-hydroxylase, physical barrier simulation, peritoneal tissue-resident macrophages, METosis-related MPO expression and activity, UVB exposure, M1 macrophage-associated iNOS activity

1 Introduction

Vitamin D (VD), recognized both as a vitamin and pre-hormone, assumes a crucial role in diverse physiological processes. Its active form, 1,25-dihydroxyvitamin D_3 (1,25(OH)$_2D_3$), is integral for bone health and calcium balance (1, 2). Although conventionally linked to calcium metabolism and skeletal well-being, recent studies have uncovered its role as an immunomodulator (3).Various immune cells, including macrophages (4), express the vitamin D receptor (VDR), a nuclear receptor and ligand-activated transcription factor belonging to the superfamily of nuclear receptors (5). Notably, macrophages not only respond to vitamin D but also possess the ability to produce bioactive vitamin D (6).

The circulating form of vitamin D, 25-hydroxyvitamin D (25 [OH]D), is predominantly bound to the vitamin D-binding protein (DBP) in the bloodstream, while 10–15% is bound to albumin, and less than 1% of circulating vitamin D exists in an unbound form (7). This binding stabilizes 25(OH)D, prolongs its half-life, and facilitates its delivery to target cells. The DBP25(OH)D complex interacts with specific receptors on the cell surface, such as megalin and cubilin, enabling endocytosis and internalization of the complex (8, 9). Inside the cell, 1,25(OH)$_2D_3$ binds to the VDR, located in either the cytosol or the nucleus. The activated VDR then forms a heterodimer with the retinoid-X receptor (RXR), which binds to DNA, thereby stimulating the production of antibiotic peptides like cathelicidin and β-defensin (10). Moreover, it is important to note that, unlike other steroid hormones in the body, which are synthesized directly from cholesterol, vitamin D synthesis requires both the 7-dehydrocholesterol precursor and UVB rays (290–320 nm) (11). In the absence of this reaction, humans must rely on dietary vitamin D intake, available in two forms: vitamin D_2 (ergocalciferol) and vitamin D_3 (cholecalciferol) (12, 13).

UVB at the Earth's surface is influenced by various physical and temporal factors, including latitude, altitude (14), season (12), and weather conditions. Biological factors, such as skin melanin (13), and personal, cultural, and behavioral factors including clothing

(15), holiday habits (16), and sunscreen use (17) as well as the extent of exposed body surface area (18), also affect the efficiency of UVB penetration, its interaction with skin cells for vitamin D synthesis, and the subsequent bioconversion process.

Moreover, it is of great importance to note that based on association studies, it has been reported that vitamin D intake, as well as circulating levels of 25(OH)D, are not systematically altered in certain pathological conditions, including autoimmune diseases, allergies, and other immune-related disorders. Conversely, insufficient vitamin D intake or reduced circulating levels have been detected in individuals who appear to be in good health. These observations emphasize that circulating 25(OH)D levels, although commonly used as standard indicators, may not be sufficient to fully assess the status of vitamin D and its role in both pathological and healthy contexts. These variations suggest that additional factors, such as differences in sun exposure, diet, or genetic capacity to metabolize vitamin D, as well as the possible presence of compensatory mechanisms, may influence the utilization and metabolism of vitamin D, including its conversion into the bioactive form, *i.e.*, $1,25(OH)_2D_3$. It is likely that these compensatory mechanisms function normally in healthy conditions but may be altered in pathological contexts.

All these observations highlight the need to study the 'active reservoir' form of vitamin D, which is ready to be utilized (when necessary) in response to external stimuli, such as activation by inflammatory factors, rather than focusing exclusively on its circulating levels. This vitamin D form could correspond to 'non-circulating vitamin D (tissue $25(OH)D_3$ levels)', produced locally in keratinocytes under the influence of UVB rays and directly used by local immune cells, such as tissue-resident macrophages. In this way, it would play an essential and direct role in modulating the immune response, compensating for the effect of circulating vitamin D deficiency. This form is not found in the bloodstream, but could be crucial for the local functions of immune cells. Here, we hypothesize that tissue-resident macrophages could be influenced by UVB exposure. This hypothesis is based on two aspects: first, their capacity to reprogram their cholesterol metabolism upon activation and exposure to inflammatory signals (19); and second, their involvement in the synthesis of bioactive molecules, including vitamin D metabolites, serving as a source of extrarenal production of $1,25(OH)_2D_3$ (20). Based on the aforementioned, this pioneering study aims to evaluate the impact of UVB radiation and passive physical barrier on both the intracellular conversion of $25(OH)D_3$ and the overall functional activities of tissue-resident macrophages.

2 Materials and methods

This study aims to assess the impact of UVB radiation and the potential influence of passive physical barriers on the enzymatic conversion activity of $25(OH)D_3$ and the overall functional activities of tissue-resident macrophages, as illustrated in the flowchart (Figure 1). Assays were conducted on whole cells, supernatants, or whole cell lysates.

2.1 Cell-based experimental model

In our study, we used murine peritoneal tissue-resident macrophages (PRMφs) as an experimental model, given their ability to metabolize $25(OH)D_3$ to $1,25(OH)_2D_3$ (21), their higher stability (22), their high responsiveness to inflammatory signals, their capacity to migrate to the skin (23) along avascular routes under inflammatory conditions (24), their role in regulating inflammation (25), their ease of accessibility, their remarkable functional plasticity, and their well-established involvement in immune responses comparable to tissue-resident macrophages in other organs. Additionally, their structural and developmental similarities with other tissues, such as the skin—including comparable surface area, mesodermal origin (26), and a shared embryonic coelomic cavity—further support their relevance in studying local immune modulation. Moreover, it is not merely because normal skin lacks a sufficient number of macrophages for planned assays, but more specifically because PRMφs are commonly used for *in vitro* assays, as they are distinguished by their maturity compared to other macrophage populations, characterized by enhanced stability in their phenotype and functionality (27).

Although the tissue was sourced from *Wistar* rats, a nocturnal species (28) that naturally displays circadian variations in metabolic and hormonal activity, the *in vitro* nature of our model allows us to minimize systemic circadian influences and focus on direct cellular responses to UVB exposure. Nonetheless, we acknowledge that macrophages possess intrinsic circadian clockworks that can remain functional even *ex vivo* (29, 30), suggesting that some degree of circadian imprinting might persist at the cellular level. While this influence is expected to be limited under controlled culture conditions, it remains an important factor to consider and explore in future *in vivo* studies.

2.2 PRMφs collection and preparation

The experiments were performed on primary PRMφs isolated from healthy 8-week-old female *Wistar rats* weighing 60–70 grams, with four independent repetitions (n = 12 per group), each conducted in duplicate or triplicate. To obtain PRMφs, peritoneal exudate cells (PECs) were collected from animals (31) in a sterile manner from the peritoneal cavity at different time intervals through lavage using a minimum of 10 mL sterile ice-cold phosphate-buffered saline (PBS) twice. This was achieved by intraperitoneal injection, followed by gentle abdominal massage, in accordance with established procedures as outlined elsewhere (32–35). PEC were seeded at 2×10^6 cells/mL in cell culture media and incubated for 2 h at 37°C in a humidified atmosphere containing 5% CO_2. The culture medium was changed regularly to maintain cell health. Non-adherent cells were removed by washing vigorously three times with warm RPMI-1640 medium. To activate PRMφs, adherent cells were incubated with 10 ng/mL LPS (*Escherichia coli* O26:B6, Sigma-Aldrich, St. Louis, MO, USA) in RPMI-1640 culture medium, supplemented with 10% fetal bovine serum (FBS), 100 U/mL penicillin, and 100 µg/mL streptomycin. Cell

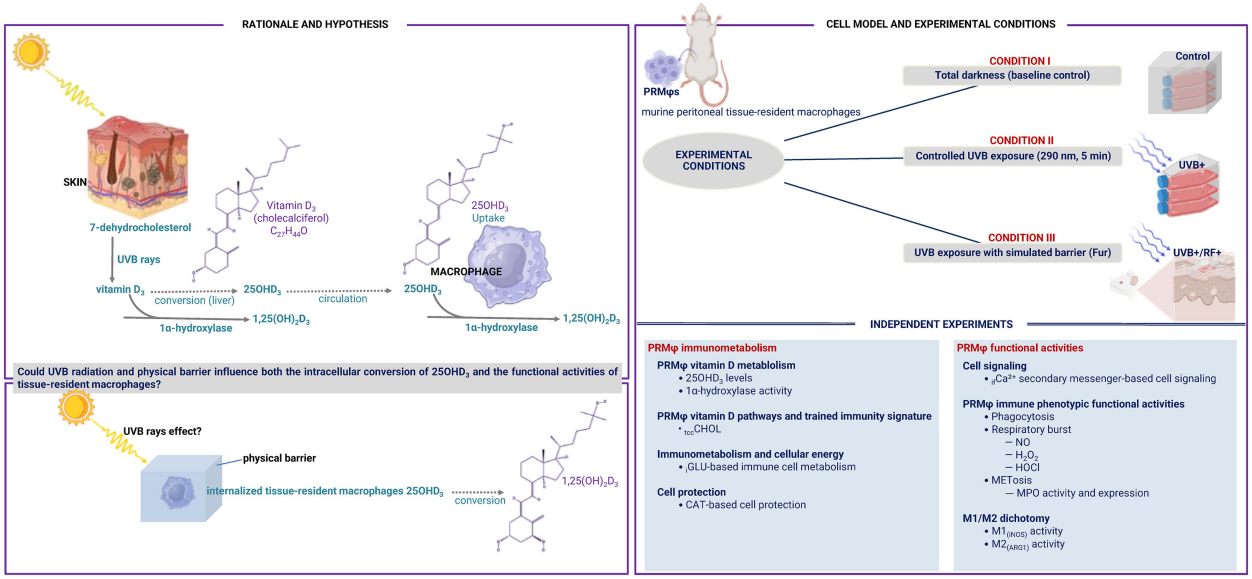

FIGURE 1
Flowchart of the current study. This study investigated the role of UVB radiation and the potential influence of passive physical barriers, such as simulated clothing, in preventing UVB exposure, on the enzymatic conversion of 25-hydroxyvitamin D3 (25(OH)D3) by 1-alpha hydroxylase, and assessed their effects on the phenotypic functional activities of tissue-resident macrophages. Experiments were conducted using murine peritoneal tissue-resident macrophages under three conditions: (i) Baseline (Control group), (ii) Controlled exposure to UVB rays (UVB+ group), and (iii) UVB exposure with a simulated physical barrier (RF+ group).

population density and viability were evaluated using the trypan blue exclusion test (TBET) with a hemocytometer under photonic microscopy (Zeiss, Jena, Germany) (36). Cell viability percentage was calculated using the standard formula: $\text{Viability}(\%) = \left(\frac{\text{Number of viable cells}}{\text{Total number of cells}}\right) \times 100$. After the adhesion step, the purity of PRMφs was analyzed using a Floid Cell Imaging Station (Thermo Fisher Scientific, MA, USA), routinely achieving a purity greater than 90%.

2.3 Experimental groups and light and barrier conditions

The experiments were conducted under three conditions:

1. **Control group:** This group was used to assess baseline levels of 25(OH)D_3, its conversion by 25-hydroxyvitamin D3-1α-hydroxylase, and overall PRMφ functional activities in the absence of light exposure.
2. **Controlled exposure to UVB rays (UVB+ group):** This group underwent a 5-min exposure to UVB radiation to mimic sunlight exposure (37), using a UV lamp calibrated to emit biologically relevant wavelengths at 290 nm.
3. **UVB exposure with a simulated physical barrier (RF+ group):** In this group, a thin layer of rat fur was placed above the cell culture system to partially mimic the passive barrier on the skin, assessing the impact of clothing-like coverage on UVB-mediated vitamin D metabolism and its effects on macrophage activity.

2.4 Rationale for the selected passive physical barrier

The use of *Wistar* rat fur was selected due to its unique physical characteristics, making it a more suitable model for our experimentation. Unlike humans, rats, as animals, do not wear clothing in their natural environment, rendering their fur a functional equivalent for protection against external elements, including UV rays. Furthermore, the choice of *Wistar* rat fur was specifically aligned with the source of the studied macrophages, which were derived from *Wistar* rats, ensuring biological consistency in the experimental setup.

Moreover, *Wistar* rat fur, due to its density and texture, could provide a relatively homogeneous and passive physical barrier that might realistically simulate skin protection against UVB rays. Unlike textiles, which vary widely in composition (e.g., synthetic *vs.* natural fibers), weave density, and industrial treatments (38–42), rat fur offers a reproducible, endogenous, and uniform material. Its fibrous structure could provide a consistent and quantifiable light-attenuating interface that partially mimics some clothing while avoiding confounding factors introduced by textile variability. This natural barrier might possess light-filtering properties akin to clothing, with the added advantage of being more easily quantifiable and manipulable in a controlled environment. Its fibrous composition also allows partial diffusion of UVB rays, which could be essential for studying the impact of reduced sun exposure on vitamin D metabolism and macrophage activity. Furthermore, the structure of the fur might replicate an effective physical barrier comparable to that of some clothing while being

less susceptible to variations inherent in different fabric types, as would be the case with conventional garments. Notably, since rats (including albino *Wistar* strains) are nocturnal (43, 44) and not naturally exposed to prolonged sunlight, their fur may incidentally limit UV radiation penetration. However, this is likely a byproduct of its primary functions (e.g., insulation) rather than a specific photoprotective adaptation—similar to how human hair (which provides both physical shading and an additional effect due to pigmentation that enhances UV absorption) can passively protect against both UVB and UVA radiation (45). Taken together, these considerations underscore the relevance of using *Wistar* rat fur as a passive physical barrier in our experimental model. Its consistent structure, endogenous origin, and natural light-attenuating properties provide a biologically and mechanically appropriate means to simulate reduced exposure to environmental stressors—including UV radiation—while ensuring reproducibility and relevance to the source of the studied macrophages.

2.5 Immune cell lysis assay

Cells were lysed for protein, $_{tcc}$CHOL, H_2O_2, and arginase activity assays. Briefly, cells were detached from culture plates, and the cell pellets were lysed using 500 µL of 0.1% Triton X-100 and incubated for 30 min. A mixture of Tris-HCl and $MnCl_2$ was added to stop the reaction, and the lysate was collected (46).

2.6 Total protein assay

Protein concentration in the cell lysates was spectrophotometrically measured at 540 nm using a commercial kit (Thermo Fisher Scientific, Inc., Middletown, CT).

2.7 25(OH)D_3 assay

Cellular vitamin D 25(OH)D_3 levels were measured using a chemiluminescent microparticle immunoassay (CMIA) on the ARCHITECT 8200 autoanalyzer (ABBOTT®) at the Biochemistry Department of Tlemcen University Hospital Center. Due to the low volume of the PRMφ culture supernatant, a volume-adjusted serum with a known concentration of vitamin D was used to ensure detectability, and the vitamin D concentration in the supernatant alone was then determined by subtracting the serum concentration from the total measured concentration.

2.8 1α-hydroxylase activity based-25(OH)D_3 bioconversion assay

To measure PRMφ 1α-hydroxylase activity, we incubated cell lysates with serum containing a known concentration of 25(OH)D_3 for two distinct time periods—30 min and 2 h, using the two-point technique (47, 48). After each incubation period, we measured the concentration of 25(OH)D_3 in the mixture. The activity of 1α-hydroxylase was calculated by determining the change in 25(OH)D_3 concentration over time and normalizing this change by the amount of protein in the sample and the time interval, using the following formula: $1\alpha - hydroxylase\ activity = \frac{[25(OH)D_3]_{initial} - [25(OH)D_3]_{final}}{t \times P}$, where t represents the incubation time and P the amount of protein in the sample (in milligrams). This approach assumes that the decrease in 25(OH)D_3 correlates with the production of 1,25(OH)$_2$$D_3$, providing an estimate of the enzyme activity based on its effect on the substrate concentration.

2.9 PRMφs functional phenotypic activities

The functional phenotypic activity of PRMφs was assessed by phagocytosis, respiratory burst activity, and METosis-related MPO expression and activity.

2.9.1 ROS-dependent NBT-based functional phagocytosis assay

The phagocytosis activity was evaluated using the nitro-blue tetrazolium (NBT, Sigma-Aldrich, Germany) assay, as previously described (49, 50). This semi-quantitative test measures the ability of phagocytic cells to reduce NBT to formazan, a black-blue crystal precipitate, reflecting the production of superoxide (O_2^-) during phagocytosis (51). To perform the assay, 100 µL of cell suspension was mixed with 100 µL of NBT solution, followed by incubation for 15 min at 37°C and an additional 15 min at room temperature, allowing the formation of formazan crystals within phagocytes. The extent of phagocytosis was quantified by measuring the reduction of soluble yellow NBT dye to insoluble black-blue formazan crystals within each PRMφs, using the Optika Microscope Camera and the Java-based image analysis software Fiji/ImageJ2 (NIH, USA). The level of phagocytosis was expressed as the percentage of NBT-positive cells.

2.9.2 Respiratory burst assay

Oxidative/respiratory burst was performed by measuring NO production, H_2O_2 levels (52), and HOCl levels (53).

a) NO assay

NO production levels were spectrophotometrically determined on supernatants based on the sensitive colorimetric Griess reaction measuring the accumulation of oxidative metabolites (NOx, nitrite [NO_2-] and nitrate [NO_3-]). The assay involved the use of vanadium chloride (III) (VCIII), and Griess reagent (Sigma-Aldrich, St. Louis, MO, USA). First, 50 µL of supernatants from the PRMφs culture was seeded into 96-well microtiter plates with 50 µL VCIII (8 mg/mL) and 25 µL of Griess reagent. The absorbance was read at 540 nm using the ELISA plate reader (Biochrom Anthos 2020, Cambridge, UK). After 30 min incubation at 37°C, concentrations of NOx were determined from a linear standard curve established by 0–150 µmol/L sodium nitrite ($NaNO_2$).

b) H_2O_2 assay

H_2O_2 levels were measured by the adapted method of Pick and Keisari. This method consists of the use of a buffered Phenol Red

Solution (PRS), which contains a peroxide assay buffer (PAB) (5.0 mM K_2HPO_4, 1.0 mM KH_2PO_4, 140 mM NaCl, 0.5 mM glucose adjusted to pH 7.4), 0.28 mM (0.1 g/L) of phenol red (phenolsulfonphthalein) and 8.5 U/L (50 µg/mL) of horseradish peroxidase (HRPO, EC 1.11.1.7). The PRS solution was prepared immediately prior to the assay, by adding phenol red and HRPO to 2.1 mL of PAB at a final concentration of 0.46 mM and 0.046 U/mL, respectively. The supernatant was added to the assay mixture at a ratio of 1 to 4 and then incubated for 30 min at 37°C. To stop the reaction, 10 µL of 1 N NaOH was added. The H_2O_2 levels were measured spectrophotometrically at 610 nm against a blank containing buffered PRS and NaOH at the appropriate concentrations. A standard curve was prepared by the use of sequential dilutions of 30% H_2O_2. Concentration of H_2O_2 was expressed as nmol per 2×10^5 cells per mL (54).

c) HOCl assay

The levels of HOCl were determined in cell supernatants by measuring the decomposition of H_2O_2 based on the *in vitro* oxidation of bromide (Br) by HOCl produced by the activated cells in the presence of chloride anion (Cl^-) released into the extracellular medium. Therefore, 10 µL of cell supernatant in PBS was added to 10 µL of 22 mM sodium bromide (NaBr). The concentration of HOBr was determined by measuring its absorbance at 330 nm immediately after 30 min and 1 h of incubation (pH 12, ε_{330} = 332 $M^{-1}cm^{-1}$) (55). The level of HOCl was estimated using a standard prepared under the same conditions by adding 10 µL of 22 mM NaBr to 10 µL of 20 mM HOCl in PBS (pH 7.4) (56–58).The values were obtained using a standard curve created by serial dilutions of 5.25% (w/v) HOCl in PBS at pH 7.4.

2.9.3 METosis-related MPO expression and activity assays

Myeloperoxidase (MPO, E.C.1.11.1.7) activity was assessed as a critical marker for the creation of macrophage extracellular traps (METs) (58). It was quantified using both a direct catalytic activity and immunofluorescence assays. For the catalytic activity assay, HOCl values were normalized to total protein content (59), with one unit of MPO activity defined as the amount catalyzing 1 µmol of HOCl per milligram of protein per 60 min and expressed percentage active chlorine per milligram of protein per one hour. The MPO expression was assessed by immunofluorescence assay based on the use of an anti-MPO antibody labeled with FITC (clone 5B8, Ms IgG1, BD Biosciences) for direct detection, performed on the Floid Cell Imaging Station (Thermo Fisher, MA, USA). CellProfiler 4.2.6 (Broad Institute, USA) was used to visualize the input image, delineate the contours of the MPO-marked fluorescent cell, segment the entire fluorescent cell, measure pixel intensity, and then calculate the area and perimeter of the MPO-marked cell. To ensure accurate comparisons and account for differences in cell size, normalized fluorescence intensity (NFI) was calculated as the weighted mean intensity (WMI) divided by the cell area (μm^2), providing a measure of fluorescence intensity per unit area, and expressed as a.u./μm^2.

2.10 M1/M2 dichotomy

The $M1_{(iNOS)}/M2_{(ARG1)}$ dichotomy was determined mathematically by measuring the M1-to-M2 ratio (60, 61).

a) $M1_{(iNOS)}$ activity assay

iNOS (EC 1.14.13.39) activity was determined by normalizing the concentration of NO to the amount of protein per well, and the results were expressed as pmol per mg of protein per 30 min (62).

b) $M2_{(ARG1)}$ activity assay

Arginase 1 activity (ARG1, EC 3.5.3.1) was assessed by a spectrophotometric assay based on evaluating the concentration of urea in PRMφs lysates after the addition of L-arginine (63). Firstly, 25 µL of cell lysates were inactivated by heating for 10 min at 56°C, then mixed with 200 µL aliquot of arginine buffer (10 mM L-arg, pH 6.4), and incubated at 37°C for 1 h. The reaction was stopped by adding acetic acid. The concentration of urea generated after arginine catabolism by arginase was measured at 600 nm (64). ARG1 activity was expressed as nanomoles of urea released per mg of proteins per 1 h (46).

2.11 CAT-based cell protection assay

CAT (EC 1.11.1.6) activity was determined by spectrophotometric analysis of H_2O_2 decomposition. Fifty microliters of cell lysates were combined with 50 µL of H_2O_2 and 50 µL of physiological saline. After vortexing and a 5-min incubation, 500 µL of titanium sulfate ($TiSO_4$) was added and vortexed. Absorbance at 420 nm was then measured, using a blank of physiological saline and $TiSO_4$.

2.12 Trained immunity activation-based $_{tcc}$CHOL signature assay

$_{tcc}$CHOL levels were measured spectrophotometrically in cell lysates by cholesterol oxidation. Free cholesterol was obtained from cholesterol esters using cholesterol ester hydrolase (EC 3.1.1.1.13), and the resulting H_2O_2 was detected at 505 nm with a chromogenic reagent (4-AP) in the presence of peroxidase (Trinder's reaction). Results were expressed as µg $_{tcc}$CHOL per mg protein.

2.13 $_i$GLU-based immune cell metabolism assay

Intracellular glucose ($_i$GLU) levels were determined spectrophotometrically in cell lysates, following supernatant removal, based on the oxidation of glucose by glucose oxidase (Gox, EC 1.1.3.4), which produces gluconic acid ($C_6H_{12}O_7$) and H_2O_2, detected at 505 nm using Trinder's method (65). The $_i$GLU concentration was calculated by comparing the absorbance to a glucose standard curve and expressed as nanomoles per mg of protein.

2.14 $_{if}Ca^{2+}$ secondary messenger-based cell signaling assay

Intracellular free calcium ions ($_{if}Ca^{2+}$) levels were measured in cell culture lysates after the removal of supernatants using the ortho-cresolphthalein complexone (o-CPC) method as described in detail (63, 66, 67), and expressed as μg/mg of protein.

2.15 Statistical analyses

Data are presented as mean ± standard error of the mean (SEM). Statistical analyses were conducted using SPSS software version 26.0 for Windows (SPSS Inc., Chicago, IL, USA). The Kruskal-Wallis test, a non-parametric method appropriate for non-normally distributed data, was used for comparisons involving more than two groups. For normally distributed data, one-way ANOVA was applied (68). Additionally, pairwise comparisons were conducted using the Student's *t*-test. A *p*-value of less than 0.05 was considered statistically significant.

3 Results

This study investigates the impact of UVB radiation and passive physical barriers on PRMφs, focusing on their effects on the enzymatic conversion of 25(OH)D_3 into its active form, 1,25(OH)$_2D_3$, mediated by 1-alpha hydroxylase, as well as their broader influence on the global functional activities of these macrophages.

3.1 UVB exposure has no effect on 25(OH)D_3 levels, but downregulates 1-alpha hydroxylase activity with the greatest impact in the simulated barrier

The results presented in Figure 2 reveal that there were no significant differences in the levels of 25(OH)D3 across the three experimental groups, irrespective of whether the PRMφs were exposed to UVB radiation alone or UVB radiation with a simulated barrier (RF + group). In contrast, Figure 3 highlights a significant downregulation in the activity of 1-alpha hydroxylase following UVB exposure. Notably, this downregulation was most pronounced in the simulated barrier group (UVB+/RF+) (for all comparisons, $p < 0.001$).

3.2 UVB increases NO production, H_2O_2, METosis-related MPO expression, and HOCl levels, with a moderate effect on phagocytosis, while the simulated barrier downregulates HOCl levels

As shown in Figure 4, UVB exposure led to a minimal increase in phagocytic activity in PRMφs, and did not reach statistical significance. In contrast, UVB exposure—whether with or without the simulated barrier—resulted in a significant upregulation of both NO and H_2O_2 levels relative to the control group ($p < 0.05$ and $p < 0.01$, respectively). Moreover, the levels of HOCl were significantly upregulated in the UVB-exposed PRMφ group ($p < 0.001$); whereas, in the RF+ group, where UVB exposure was combined with a simulated barrier, HOCl levels returned to baseline levels, showing no significant difference when compared to the control group (for the comparison among the three groups using ANOVA, $p < 0.001$).

Figure 5 further extends our analyses by specifically exploring MPO activity and expression. The analysis of MPO fluorescence intensity highlighted significant differences across the three experimental groups, underscoring the impact of UVB exposure on PRMφ activation. In contrast to the control group, where the fluorescence intensity corresponded to minimal MPO expression levels, the PRMφs group exposed to UVB displayed the highest fluorescence intensity, corresponding to the significant upregulation of MPO expression, likely triggered by UVB-induced stimulation. Lastly, in the RF+ group, where a simulated barrier limited UVB exposure, the fluorescence intensity remained similar to baseline levels. This suggests that while fluorescence intensity increased per unit area, the overall effect of UVB on METosis-related MPO activity was substantially attenuated by the simulated barrier. These findings were consistent across normalized fluorescence intensity ($p < 0.001$ by ANOVA test), area ($p < 0.001$ by Kruskal-Wallis test), perimeter ($p < 0.01$ by Kruskal-Wallis test), and normalized weighted mean intensity of MPO-marked cells ($p < 0.001$ by ANOVA test), further corroborated by the direct enzymatic activity analysis of MPO ($p < 0.001$ by ANOVA test).

3.3 UVB upregulates iNOS activity and shifts $M1_{(iNOS)}$/$M2_{(ARG1)}$ towards M1 functional phenotype

Figure 6 illustrates the effects of UVB exposure on the enzymatic activity of iNOS and ARG1 in PRMφs, revealing distinct modulatory patterns. Unlike iNOS activity, ARG1 activity was significantly downregulated in PRMφs exposed to UVB radiation ($p < 0.01$). The passive physical barrier similarly reduced ARG1 activity, though this effect was less pronounced compared to UVB exposure ($p < 0.05$). In contrast, neither UVB radiation nor the physical barrier significantly altered iNOS activity. Finally, both the UVB-exposed group and the RF+ group exhibited a significant increase in the $M1_{(iNOS)}$-to-$M2_{(ARG1)}$ ratio, indicating a shift toward a more M1-like phenotype ($p < 0.01$ by ANOVA test).

3.4 UVB downregulates CAT activity, specifically in simulated barrier condition

As shown in Figure 7, UVB exposure induced a significant downregulation of CAT activity in PRMφs. This activity decreased even further in the PRMφ group with the simulated barrier (RF+

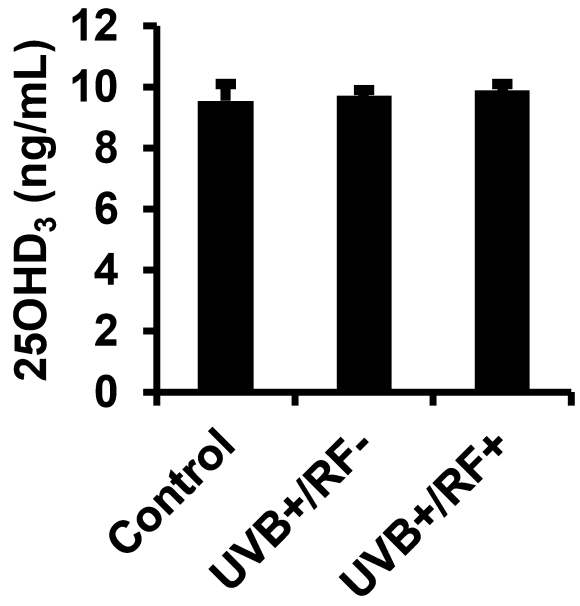

FIGURE 2
Effects of UVB radiation and passive physical barrier on 25(OH)D_3 content of PRMφs. Experiments were conducted on murine peritoneal tissue-resident macrophages (PRMφs) under three conditions: (i) Control group, (ii) Controlled exposure to UVB rays (UVB+ group), and (iii) UVB exposure with a simulated physical barrier (RF+ group). Levels of 25(OH)D_3 were measured using a chemiluminescent microparticle immunoassay. Data are presented as mean ± standard error of the mean (SEM) from four independent repetitions (n = 12 per group). No significant differences were observed between groups using one-way ANOVA.

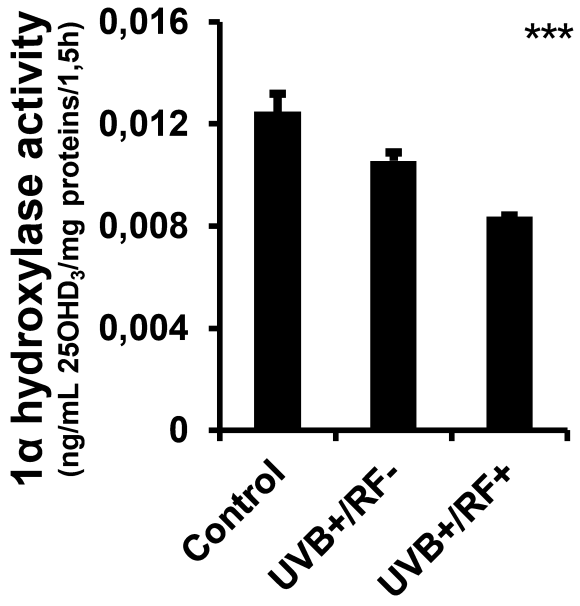

FIGURE 3
Effects of UVB radiation and passive physical barrier on 25-hydroxyvitamin D_3-1alpha-hydroxylase of PRMφs. Experiments were conducted on murine peritoneal tissue-resident macrophages (PRMφs) under three conditions: (i) Control group, (ii) Controlled exposure to UVB rays (UVB+ group), and (iii) UVB exposure with a simulated physical barrier (RF+ group). The activity of 1α-hydroxylase assay was based on the two-point technique, determining the change in 25(OH)D_3 concentration over time and normalizing this change by the amount of protein in the sample and the time interval. Data are presented as mean ± standard error of the mean (SEM) from four independent repetitions (n = 12 per group). Significant differences are indicated by an asterisk. Statistical analyses were performed using one-way ANOVA. ***$p < 0.001$.

group) compared to the control group. For multiple comparisons using ANOVA test, p-value was less than 0.001.

3.5 Simulated barrier attenuates the UVB-induced increase in $_{tcc}$CHOL

As shown in Figure 8, $_{tcc}$CHOL levels were upregulated in the UVB-exposed PRMφ group compared to the control PRMφ group, although the difference was not statistically significant. However, in the RF+ group, where UVB exposure was combined with a simulated barrier (rat fur), $_{tcc}$CHOL levels returned to near baseline values. For all comparisons between the three groups using the Kruskal-Wallis test, the p-value was less than 0.05.

3.6 UVB decreases $_{i}$GLU levels with a more pronounced effect under the simulated barrier condition

Figure 9 illustrates that UVB radiation, regardless of whether combined with the simulated barrier (UVB+/RF+ group) or not (UVB+/RF- group), led to a significant downregulation in $_{i}$GLU levels compared to the control PRMφ group. Notably, the decrease in $_{i}$GLU levels was more pronounced in the UVB+/RF+ group (p-value was less than 0.001 using ANOVA test), suggesting that the presence of the simulated barrier may enhance or reinforce this effect.

3.7 UVB exposure alone does not alter $_{if}Ca^{2+}$ levels, but a mild increase is observed with the simulated barrier

As shown in Figure 10, there were no significant differences in $_{if}Ca^{2+}$ levels among the three experimental groups. However, the UVB-exposed PRMφ group with the simulated barrier (UVB+/RF+) showed an upregulation in $_{if}Ca^{2+}$ levels, although this increase was not statistically significant, suggesting a subtle enhancement of calcium signaling by the simulated barrier.

4 Discussion

Tissue macrophages act as immune sentinels due to their strategic positioning and ability to initiate and modulate immune responses during infection or injury, while maintaining tissue homeostasis (69–71). Among these, peritoneal macrophages are well-characterized in terms of development, biology, and inflammation-related responses (72–76).

10.3389/fimmu.2025.1583493

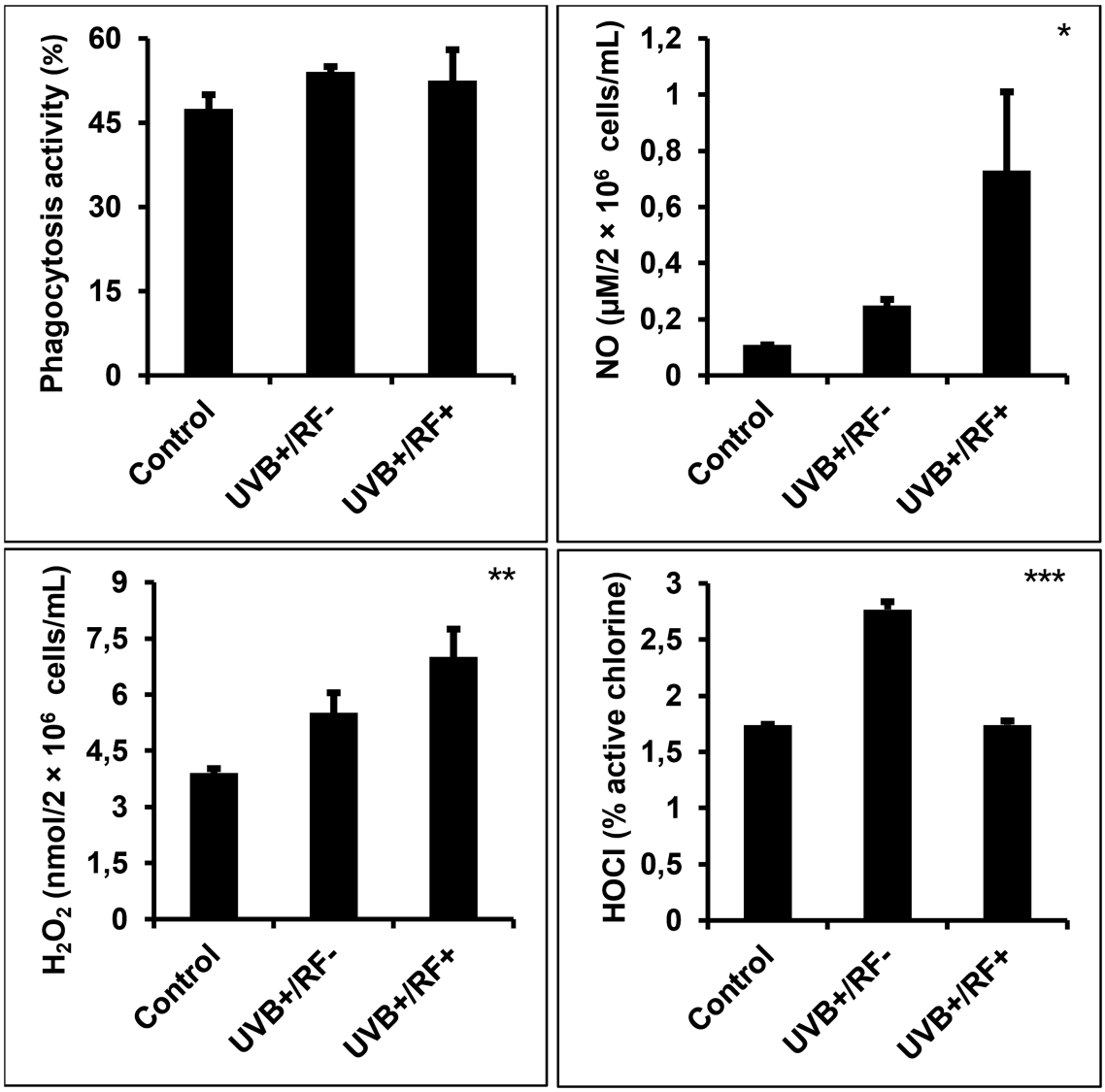

FIGURE 4
Effects of UVB radiation and passive physical barrier on phagocytosis and respiratory burst activity of PRMφs. Experiments were conducted on murine peritoneal tissue-resident macrophages (PRMφs) under three conditions: (i) Control group, (ii) Controlled exposure to UVB rays (UVB+ group), and (iii) UVB exposure with a simulated physical barrier (RF+ group). Phagocytosis activity was evaluated using the NBT method, based on its reduction to formazan by superoxide anions produced during the respiratory burst in phagocytic cells. Oxidative/respiratory burst was performed by measuring the levels of NO production, H_2O_2 levels, and HOCl. H_2O_2 levels were spectrophotometrically determined using a phenol red-based assay. NO production levels were spectrophotometrically determined using the sensitive colorimetric Griess method. HOCl levels were determined by measuring the decomposition of H_2O_2 through *in vitro* bromide oxidation by HOCl generated by activated cells in the presence of chloride released into the extracellular medium. Data are presented as mean ± standard error of the mean (SEM) from four independent repetitions (n = 12 per group). H_2O_2: hydrogen peroxide, HOCL: hypochlorous acid, NBT: nitro-blue tetrazolium, NO: nitric oxide. Significant differences are indicated by an asterisk. Statistical analyses were performed using one-way ANOVA. $^*p < 0.05$, $^{**}p < 0.01$, $^{***}p < 0.001$.

While UVB exposure from natural or artificial sources is known to modulate immunity locally and systemically, typically reducing cellular responses (77–79), our study is, to our knowledge, the first to examine how UVB radiation and passive physical barriers affect both intracellular $25OHD_3$ conversion and functional characteristics of tissue-resident macrophages under the studied conditions.

Although it might initially seem intuitive that introducing a passive physical barrier would simply attenuate UVB-induced inflammation by reducing exposure intensity, our results suggest a more nuanced and biologically significant phenomenon. The presence of a fur-based barrier did not merely lower UVB energy input, but qualitatively modulated key aspects of the macrophage response. Specifically, we observed changes in macrophage polarization (M1/M2), enzymatic activity (iNOS, MPO, Arg1), phagocytic function, and the expression of local 1α-hydroxylase involved in vitamin D activation. These findings indicate that the passive barrier influenced not only the total UVB dose but also its spectral and spatial properties—through wavelength-dependent filtering consistent with Beer–Lambert principles and modulation by light scattering. While the Beer–Lambert framework provides a

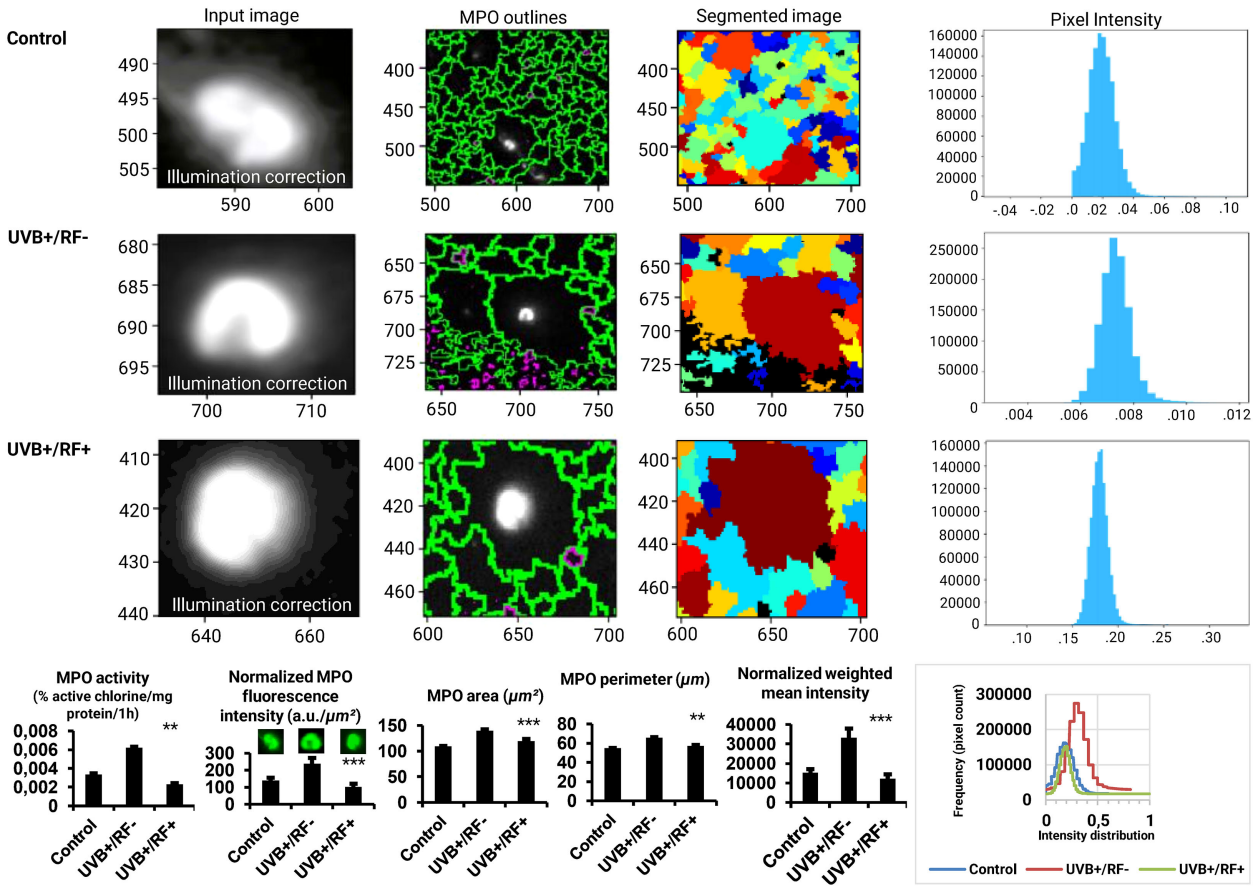

FIGURE 5
Effects of UVB radiation and passive physical barrier on MPO expression and activity of PRMφs. Experiments were conducted on murine peritoneal tissue-resident macrophages (PRMφs) under three conditions: (i) Control group, (ii) Controlled exposure to UVB rays (UVB+ group), and (iii) UVB exposure with a simulated physical barrier (RF+ group). MPO activity was quantified by directly measuring HOCl levels, normalized to total protein content, and expressed as percentage active chlorine per milligram of protein per one hour. MPO expression was assessed *via* immunofluorescence imaging, analyzed using CellProfiler software (v4.2.6, Broad Institute, USA). For imaging analysis, object dimensions were converted from pixels to micrometers (μm) to ensure accurate quantification. This conversion is based on an estimated image resolution of 0.58 μm per pixel, derived from an approximate field of view of 750 μm for an image width of 1296 pixels. The resolution was calculated as: $Resolution = \frac{Field\ of\ view\ width\ (\mu m)}{Image\ width\ (pixels)} = \frac{750\ \mu m}{1296\ pixels} \approx 0.5787 \mu m/pixel$. This estimation aligns with the theoretical resolution limit of the device (~0.5 μm). To convert area values, the square of the resolution (0.58 μm/pixel)^2 was applied to pixel measurements, resulting in approximate areas in μm^2. For perimeter values, a linear conversion of 0.58 μm/pixel was applied. Therefore, the reported values should be considered approximate. The intensity measurements were normalized using a min-max scaling approach to ensure comparability across images with differing intensity ranges. This normalization method adjusts the raw pixel intensities (I) to a scale between 0 and 1, calculated as: $I_{normalized} = \frac{I - I_{min}}{I_{max} - I_{min}}$, where I_{min} and I_{max} represent the minimum and maximum intensity values in the dataset, respectively. This process preserves the relative differences between pixel intensities while standardizing their range aligning with the quantitative expectations of the theoretical resolution limits and ensuring that the observed patterns are not influenced by varying dynamic ranges of the original images. The normalization was performed independently for each group, allowing for direct comparisons of intensity distributions across experimental conditions. Finally, the weighted mean intensity (WMI) values were calculated to account for the normalized intensity distributions across the analyzed regions of interest (ROIs). These values were derived as: $WMI = \frac{\sum_i w_i \times I_i}{\sum_i w_i}$, where I_i represents the intensity value of a given pixel, and W denotes the pixel area. This method ensures that the calculated intensity reflects the contribution of each pixel proportionally to its area within the ROI. Overlaid histograms representing the fluorescence intensity distribution for the three experimental groups. Intensities were normalized to ensure comparability, and the x-axis represents fluorescence intensities (a.u.), while the y-axis indicates the pixel count. For histogram data, values are presented as mean ± standard error of the mean (SEM) from four independent repetitions (n = 12 per group). HOCl: hypochlorous acid, MPO: myeloperoxidase, RF: rat fur, UVB: ultraviolet B. Significant differences are indicated by an asterisk. Statistical analyses were performed using the Kruskal-Wallis test for non-normally distributed data (area and perimeter) or one-way ANOVA for normally distributed data (normalized fluorescence intensity, normalized weighted mean intensity, and MPO activity). $^{**}p < 0.01$, $^{***}p < 0.001$.

basis for understanding absorption-driven attenuation, additional tissue-relevant factors such as anisotropy, optical heterogeneity, and multiple scattering—known to deviate from ideal Beer–Lambert conditions in biological systems—likely contribute to the altered UVB distribution and biological effects (80, 81). Such selective attenuation may result in change in signaling cascades within skin-resident immune cells.

In line with previous observations in tissue-specific immunomodulation, our results reinforce the notion that the local photophysical environment—including the presence of

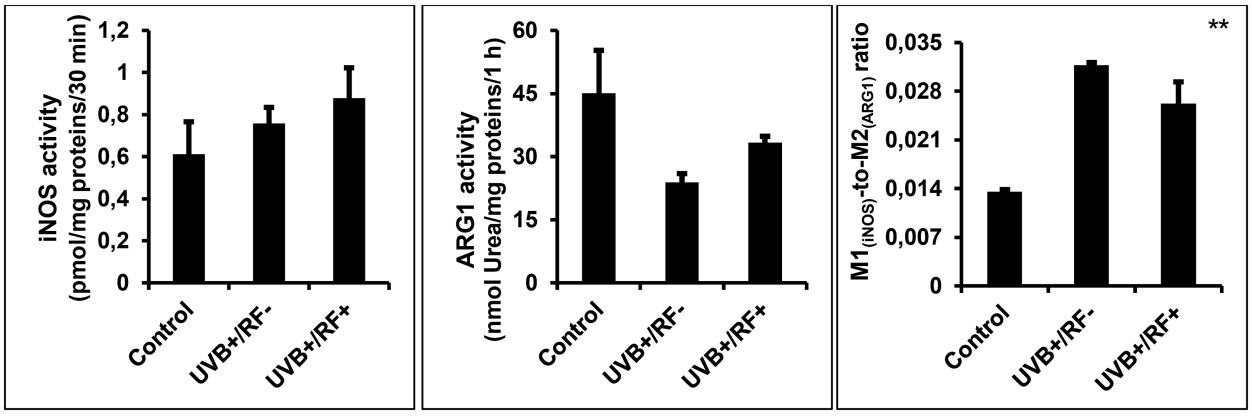

FIGURE 6
Effects of UVB radiation and passive physical barrier on the M1/M2 dichotomy. Experiments were conducted on murine peritoneal tissue-resident macrophages (PRMφs) under three conditions: (i) Control group, (ii) Controlled exposure to UVB rays (UVB+ group), and (iii) UVB exposure with a simulated physical barrier (RF+ group). The $M1_{(iNOS)}/M2_{(ARG1)}$ dichotomy was determined mathematically by measuring the M1-to-M2 ratio. M1 activity was determined by measuring iNOS (EC 1.14.13.39) activity through the quantification of NO production normalized to protein content, whereas M2 activity was assessed by measuring the amount of urea generated by ARG1 (EC 3.5.3.1). Data are presented as mean ± standard error of the mean (SEM) from four independent repetitions (n = 12 per group). iNOS: inducible nitric oxide synthase, ARG1: arginase 1. Significant differences are indicated by an asterisk. Statistical analyses were performed using one-way ANOVA. $^{**}p < 0.01$.

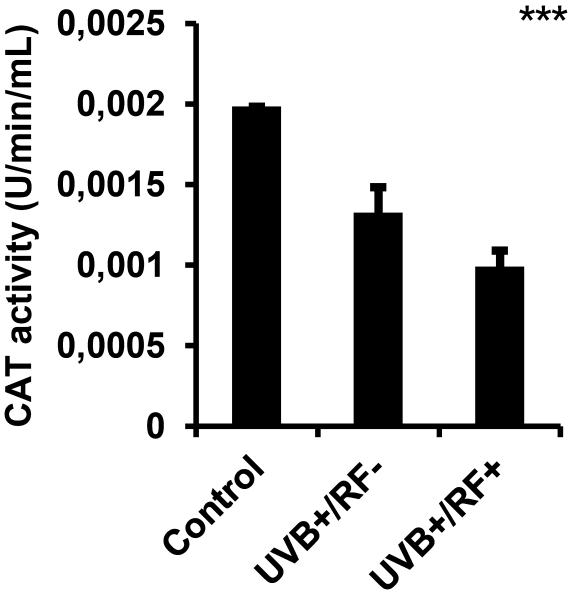

FIGURE 7
Effects of UVB radiation and passive physical barrier on catalase-based cell protection activity of PRMφs. Experiments were conducted on murine peritoneal tissue-resident macrophages (PRMφs) under three conditions: (i) Control group, (ii) Controlled exposure to UVB rays (UVB+ group), and (iii) UVB exposure with a simulated physical barrier (RF+ group). CAT (EC 1.11.1.6)-based cell protection activity was spectrophotometrically assessed by measuring H_2O_2 decomposition through titanium sulfate-based detection. Data are presented as mean ± standard error of the mean (SEM) from four independent repetitions (n = 12 per group). CAT: catalase activity, H_2O_2: hydrogen peroxide. Significant differences are indicated by an asterisk. Statistical analyses were performed using one-way ANOVA. $^{***}p < 0.001$.

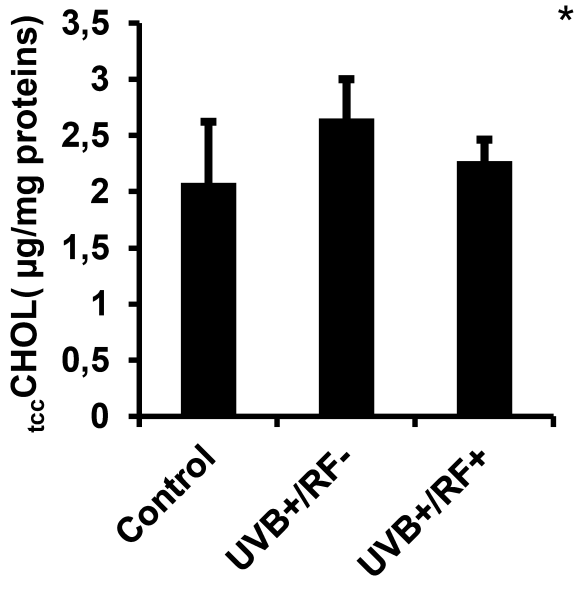

FIGURE 8
Effects of UVB radiation and passive physical barrier on trained immunity activation-based $_{tcc}$CHOL signature of PRMφs. Experiments were conducted on murine peritoneal tissue-resident macrophages (PRMφs) under three conditions: (i) Control group, (ii) Controlled exposure to UVB rays (UVB+ group), and (iii) UVB exposure with a simulated physical barrier (RF+ group). Trained immunity activation-based $_{tcc}$CHOL signature was measured spectrophotometrically through Trinder's reaction. Data are presented as mean ± standard error of the mean (SEM) from four independent repetitions (n = 12 per group). $_{tcc}$CHOL: total cellular cholesterol content. Significant differences are indicated by an asterisk. Statistical analyses were performed using one-way ANOVA. $^{*}p < 0.05$.

10.3389/fimmu.2025.1583493

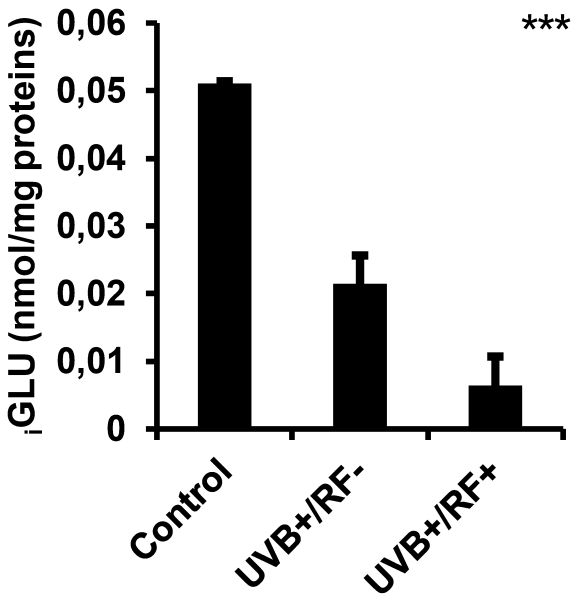

FIGURE 9
Effects of UVB radiation and passive physical barrier on ¡GLU-based immune cell metabolism of PRMφs. Experiments were conducted on murine peritoneal tissue-resident macrophages (PRMφs) under three conditions: (i) Control group, (ii) Controlled exposure to UVB rays (UVB+ group), and (iii) UVB exposure with a simulated physical barrier (RF+ group). ¡GLU-based immune cell metabolism was assessed spectrophotometrically by measuring H_2O_2 produced during glucose oxidation by glucose oxidase. Data are presented as mean ± standard error of the mean (SEM) from four independent repetitions (n = 12 per group). ¡GLU: intracellular glucose. Significant differences are indicated by an asterisk. Statistical analyses were performed using one-way ANOVA.
***$p < 0.001$.

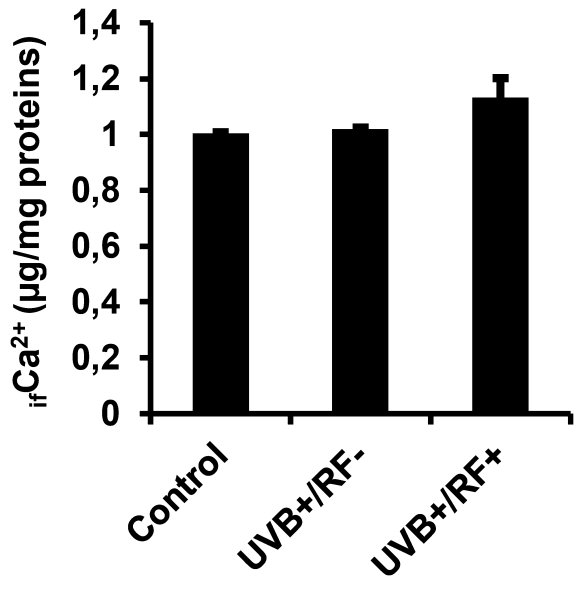

FIGURE 10
Effects of UVB radiation and passive physical barrier on free Ca^{2+} levels in PRMφs. Experiments were conducted on murine peritoneal tissue-resident macrophages (PRMφs) under three conditions: (i) Control group, (ii) Controlled exposure to UVB rays (UVB+ group), and (iii) UVB exposure with a simulated physical barrier (RF+ group). $_{if}Ca^{2+}$ levels were assessed using the ortho-cresolphthalein complexone (oCPC) method. Data are presented as mean ± standard error of the mean (SEM) from four independent repetitions (n = 12 per group). No significant differences were observed between groups using one-way ANOVA. $_{if}Ca^{2+}$, intracellular free calcium ions.

partial UVB barriers such as clothing or natural photoprotective substances (82–84)—can shape immunological outcomes in a non-linear, context-dependent manner. This distinction is clinically relevant: in autoimmune or chronic inflammatory diseases, a controlled modulation of UVB-induced macrophage activation could help limit deleterious inflammation, while in oncology or infectious contexts, preserving specific UVB wavelengths might enhance beneficial immune responses. Notably, this could extend to inflammatory bowel diseases (IBD), where systemic and local macrophage dysregulation is a known factor (85), and where skin-mediated photomodulation might exert systemic effects. Moreover, our findings may also be relevant in the context of skin inflammatory disorders such as psoriasis and atopic dermatitis, where dysregulated macrophage activation contributes to disease pathogenesis (86–90). By demonstrating that UVB exposure modulates tissue-resident macrophage function—both enhancing and restraining oxidative activity depending on barrier conditions—our study suggests that careful manipulation of UVB exposure could offer therapeutic avenues for these conditions. Further investigations in preclinical and clinical models are warranted to fully elucidate these translational possibilities.

4.1 Effects of UVB radiation and passive physical barrier on 25-hydroxyvitamin D_3-1alpha-hydroxylase of PRMφs

Our findings show that UVB significantly downregulates 1α-hydroxylase activity. This may stem from the non-enzymatic UV-driven conversion of 7-dehydrocholesterol (7-DHC) to previtamin D_3, bypassing enzymatic steps (91, 92). This aligns with the concept that metabolic pathways, including vitamin D conversion, adapt dynamically to physiological needs rather than being solely driven by circadian rhythms (93).

Supporting evidence also links vitamin D to sleep regulation: its receptor and metabolizing enzymes are expressed in sleep-regulatory brain regions (94), and vitamin D promotes melatonin synthesis—a hormone critical for circadian alignment and nocturnal physiological processes (95, 96). A systematic review in youth populations reported a link between vitamin D deficiency and disorders like insomnia, obstructive sleep apnea (OSA), and restless legs syndrome (RLS), highlighting its involvement in serotonergic/dopaminergic pathways vital to sleep (97).

Our data also show that the simulated rat barrier dampens UVB penetration, markedly reducing 1α-hydroxylase activity in the UVB +/Rat fur+ condition (18). This reinforces the concept that physical

obstructions can limit local UVB-induced vitamin D metabolism by restricting UVB access.

4.2 Effects of UVB radiation and passive physical barrier on phagocytosis and respiratory burst activity of PRMφs

Our study revealed a modest increase in phagocytic activity of PRMφs upon direct UVB exposure. In contrast, previous *in vivo* studies reported impaired macrophage function following systemic UV irradiation, including reduced phagocytosis, bacterial clearance, and NO production (98, 99). These discrepancies likely stem from differences in experimental models—namely, our direct *in vitro* exposure versus whole-body UVB irradiation, which introduces systemic and indirect immune effects. By isolating macrophages *ex vivo*, our approach reveals a cell-intrinsic enhancement of phagocytic function, avoiding confounding influences from other immune or stromal cells.

Similarly, another study (99) showed diminished phagocytosis and active oxygen production in macrophages after UVB exposure, though neutrophils were unaffected. Our approach isolated the direct impact of UVB on PRMφs, excluding systemic factors or indirect effects mediated by other cell types. This may explain why we observed a cell-autonomous increase in phagocytic activity, whereas *in vivo* studies reported broader functional impairments due to whole-body irradiation. Furthermore, while our study did not assess other immune cells, including neutrophils, the differential effects of UVB across innate immune cell types suggest that tissue-resident macrophages may be particularly sensitive to UVB-induced modulation.

Differences in UVB doses and functional assays may also contribute to conflicting results in the literature. While other studies emphasized microbial killing, we focused on NBT-based assay to assess phagocytosis, highlighting UVB-induced ROS production during this process. Notably, phagocytosis in the UVB+/RF+ group remained higher than in the control but slightly lower than in the UVB+/RF– group, suggesting that the barrier dampens—but does not abolish—UVB effects.

The respiratory burst is central to macrophage antimicrobial defense, involving ROS and RNS generation. UVB exposure increased NO and H_2O_2 levels in PRMφs, even with partial UVB attenuation by fur, supporting its capacity to stimulate innate immune responses. Our NO data are consistent with reports of UVB-induced NO production in murine PRMφs (100) and human vitiligo skin (101), but differ from studies where therapeutic UVB inhibited NOS2 expression in keratinocytes and macrophages (102). Similarly, H_2O_2 production in response to UVB mirrors findings in neutrophils (103), mouse serum (104), and even algae (105), underscoring the evolutionary conservation of this oxidative stress response.

4.3 Effects of UVB radiation and passive physical barrier on MPO expression and activity of PRMφs

Our findings show that UVB exposure significantly enhances HOCl production in PRMφs, supporting our previous results on the respiratory burst. This increase is accompanied by higher MPO expression, suggesting activation of myeloperoxidase-driven oxidative mechanisms, potentially indicating METosis-like activity. The presence of rat fur, mimicking some clothing, partially attenuated this effect, highlighting its role as a passive UVB barrier—consistent with evidence that garments reduce UVB impact on skin and immune responses (106).

Elevated MPO activity, though crucial for microbial killing, is also implicated in chronic inflammatory diseases. For example, in atherosclerosis—a persistent immunoinflammatory condition—MPO-derived oxidants contribute to tissue damage, oxidized LDL accumulation, and lesion progression (107–111). Similarly, in Crohn's disease, characterized by intestinal inflammation and immune dysregulation (112, 113), UVB-induced MPO activity may intensify oxidative stress, underlining the need to limit UVB exposure in such contexts.

Conversely, increased MPO activity in malignant conditions may support macrophage-mediated antitumor responses (114), with some studies linking higher MPO levels to reduced tumor growth and improved survival (115). This dual role suggests the context-dependent outcomes of UVB-induced MPO activation.

While rat fur differs from human fabric, it provides a consistent UVB-shielding surface. Its light-filtering properties parallel those of clothing, which varies in UV modulation based on material thickness, porosity, fiber composition, and moisture (116–120). The partial barrier function of fur may thus modulate UVB-induced inflammation without fully suppressing macrophage activity.

To assess the translational potential of our findings, future *in vivo* studies are needed to examine the systemic consequences of UVB-induced MPO activation and its modulation by passive physical barriers in disease settings. We acknowledge that our *ex vivo* model, while providing tight experimental control, does not fully recapitulate the complexity of organismal physiology. Extension to relevant *in vivo* models of chronic inflammation, cardiovascular disease, or cancer may reveal novel therapeutic applications for UVB and vitamin D–mediated modulation of macrophage function.

4.4 Effects of UVB radiation and passive physical barrier on the M1/M2 dichotomy

iNOS and ARG1 compete for L-arginine, their shared substrate, in activated macrophages. iNOS uses L-arginine to produce NO, whereas ARG1 converts it into L-ornithine and urea. Elevated

ARG1 activity can therefore limit L-arginine availability for iNOS, reducing NO production (121).

Classically activated M1 macrophages are typically associated with high iNOS expression and NO production, representing a proinflammatory phenotype (122), whereas M2 macrophages display higher ARG1 activity, contributing to immunoregulation and wound healing (123). Thus, the iNOS/ARG1 balance shapes macrophage polarization and function (124, 125).

Our results confirm that UVB exposure enhances iNOS activity in PRMφs, consistent with previous studies in immune and skin cells (100, 126–128). Simultaneously, we observed decreased ARG1 activity, aligning with reports showing reduced M2-like macrophages after moderate UVB irradiation (129, 130). This shift in the iNOS/ARG1 ratio indicates a tendency toward an M1-like polarization. This is further supported by Karisola et al. (131), who demonstrated that UVB radiation promotes proinflammatory M1 macrophages. A potential mechanism for this polarization is UVB-induced cellular stress, which may activate proinflammatory signaling pathways, such as NF-κB (132). Additionally, UVB exposure has been shown to upregulate toll-like receptor (TLR) signaling, further driving M1 polarization (133–135).

Interestingly, the presence of a simulated barrier (RF+) further enhances iNOS activity, suggesting that the barrier may influence PRMφs beyond simple UV filtration, possibly through additional mechanical or environmental cues. Further studies are needed to determine whether this shift is transient or sustained and to elucidate the underlying molecular pathways.

4.5 Effects of UVB radiation and passive physical barrier on CAT activity in PRMφs

CAT is a key antioxidant enzyme that decomposes H_2O_2 into water and oxygen, shielding macrophages from oxidative damage (136). In our study, CAT activity peaked when PRMφs were fully shielded from UVB, emphasizing its frontline role in defending against oxidative stress. Conversely, direct UVB exposure markedly reduced CAT activity, even when partially filtered by the passive physical barrier, revealing the enzyme's sensitivity to UVB-induced oxidative stress.

Beyond its role in neutralizing ROS, CAT is essential for maintaining redox homeostasis, which supports macrophage viability and function (137, 138). The observed suppression of CAT activity after UVB exposure indicates a weakened antioxidant defense, potentially impairing macrophage responsiveness and survival. Interestingly, the intermediate CAT activity observed in partially shielded cells suggests a threshold effect, where suboptimal UVB levels may not fully activate protective mechanisms yet still cause cellular damage.

These findings point to the need for further investigation into the molecular mechanisms underlying UVB-induced CAT alteration, including the potential involvement of redox-sensitive signaling pathways or epigenetic regulation. A deeper understanding of how environmental stress modulates macrophage antioxidant capacity could inform strategies for preserving immune cell function under oxidative conditions.

4.6 Effects of UVB radiation and passive physical barrier on trained immunity activation-based $_{tcc}$CHOL signature of PRMφs

Our findings show a slight increase in $_{tcc}$CHOL levels in UVB-exposed PRMφs, suggesting that UVB influences cholesterol metabolism, likely *via* oxidative stress and metabolic reprogramming. UVB-generated ROS (139–141) are known to affect enzymes like HMG-CoA reductase (142) and cholesterol efflux transporters such as ABCG1 (143), potentially disrupting cholesterol homeostasis. Interestingly, $_{tcc}$CHOL levels returned to near baseline in the RF+ group, indicating that the passive physical barrier mitigated UVB effects.

Changes in $_{tcc}$CHOL levels are also relevant to trained immunity—a long-lasting innate immune adaptation driven by metabolic and epigenetic reprogramming (144, 145). While moderate ROS can enhance trained immunity (146), excessive cholesterol accumulation may provoke dysfunction (147). Cholesterol and its metabolites shape key metabolic pathways and epigenetic remodeling, notably *via* LXR-alpha activation (148, 149), mTOR signaling (150, 151), and regulation of DNA methylation and histone acetylation. Additionally, cholesterol is an integral component of lipid rafts, which cluster PRRs like TLRs and potentiate immune signaling (152–154). Consequently, alterations in $_{tcc}$CHOL levels could impact raft integrity and PRMφ responsiveness to secondary challenges—though this remains hypothetical and warrants experimental validation.

Finally, cholesterol's role in modulating mitochondrial function and ROS production adds another layer of immune regulation (155). The normalization of $_{tcc}$CHOL in the RF+ group suggests that passive physical barriers may help maintain a balance between the beneficial aspects of trained immunity and the potentially harmful effects of oxidative stress.

4.7 Effects of UVB radiation and passive physical barrier on $_{i}$GLU-based immune cell metabolism of PRMφs

Glucose is the primary energy substrate supporting key macrophage functions (156). While its role in immune activation has long been recognized, its impact on cellular metabolism—particularly in linking energy production to immune responses—

has only recently been fully appreciated. In macrophages, glucose not only fuels ATP production *via* glycolysis and oxidative phosphorylation (OXPHOS) but, also supports essential biosynthetic processes by providing NADPH for ROS generation, glycerol 3-phosphate for lipid synthesis, and ribose for RNA synthesis required for cytokine production (157–159).

In our study, UVB exposure led to a marked decrease in $_{i}$GLU levels in PRMφs, likely reflecting an upregulation of oxidative metabolism and increased metabolic demand. This aligns with the observed rise in oxidative stress markers—including NO, H_2O_2, and HOCl—highlighting the interplay between energy metabolism and immune activation under photonic stress.

Interestingly, the simulated physical barrier further intensified the decrease in $_{i}$GLU levels. Rather than mitigating the UVB effect, the passive barrier appeared to modulate glucose metabolism—possibly by altering glucose uptake, transporter expression, or by promoting alternative metabolic pathways activated under dual stress conditions. This unexpected outcome suggests that the barrier may function not only as a physical shield that limits UVB radiation exposure, but also as a biological modulator influencing cellular metabolism in tissue-resident macrophages in PRMφs, revealing a complex interaction between environmental stressors and immune cell bioenergetics. Further investigation is needed to elucidate the underlying mechanisms and to determine whether this effect is beneficial or detrimental to macrophage function and survival.

4.8 Effects of UVB radiation and passive physical barrier on $_{if}Ca^{2+}$ levels in PRMφs

$_{if}Ca^{2+}$ serves as a pivotal second messenger controlling various macrophage functions, including phagocytosis and oxidative burst in macrophages (160–162). In our study, UVB exposure alone did not significantly alter $_{if}Ca^{2+}$ levels in PRMφs. However, a mild, non-significant increase was observed in the UVB+/RF+ group, suggesting that partial attenuation and spectral modulation by the simulated barrier may subtly enhance calcium signaling.

This subtle enhancement may reflect wavelength-dependent changes in receptor- or ion channel–mediated calcium influx, as well as possible involvement of intracellular stores through endoplasmic reticulum channels like inositol 1,4,5-trisphosphate receptor (IP_3R) and ryanodine receptor (RyR) (163), which are sensitive to ROS and calcium dynamics (164).

Additionally, mitochondrial calcium uptake *via* the mitochondrial calcium uniporter-associated channel (MiCa) channel may stimulate ATP production and ROS generation (165, 166). Since longer wavelengths can enhance mitochondrial ROS output (167–170), the spectral shift induced by the passive physical barrier—likely absorbing short UVB (292 nm) and transmitting longer wavelengths—may influence these interconnected pathways. These interlinked mechanisms are coherent with our findings of elevated NO and H_2O_2 levels, suggesting that barrier-modulated UVB exposure may fine-tune calcium signaling and oxidative stress responses in PRMφs. Future studies will be needed to clarify whether these calcium dynamics translate into functional changes under photonic stress.

4.9 Synthesis: integrated effects of UVB radiation and biological barrier on PRMφs function – spectral, energetic, and functional modulation

Our findings highlight the multifaceted impact of UVB radiation on PRMφ function, revealing that the presence of a biological barrier—simulated by rat fur—modulates both the intensity and quality of UVB reaching the cells. The barrier's partial absorption of photons not only reduces UVB intensity but also shifts the average wavelength toward longer values, thereby decreasing photon energy, as predicted by Planck's relation $E = \frac{h \times c}{\lambda}$, where h is Planck's constant, c the speed of light, and λ the wavelength (171, 172). Lower-energy photons are less effective at exciting biomolecular electrons, such as those in proteins and lipids, which dampens cellular responses to photonic stress. According to the Grotthuss-Draper law, only absorbed photons can initiate photochemical changes (173–175), implying that reduced photon energy directly modulates PRMφ activity.

Beyond simple shielding, UVB photons interact with sensitive molecular targets like transient receptor potential (TRP) channels, rhodopsins (a member of the G protein-coupled receptor [GPCR] family), and flavins (176–179), thereby influencing intracellular signaling cascades. These effects involve complex phenomena at the crossroads of optics, quantum physics (e.g., photon scattering and interference), and molecular biology. The passive barrier's selective absorption and scattering alter photon-cell interactions, potentially explaining how the barrier increases $_{if}Ca^{2+}$ levels while dampening the excitation of other pathways.

Overall, this integrated analysis underscores the dual importance of UVB intensity and spectral composition in shaping PRMφ functions. A deeper understanding of how passive physical barriers modulate photonic stress could inform strategies to preserve immune cell resilience under environmental stressors.

5 Conclusions and future prospects

Our study highlights the significant effects of UVB exposure on PRMφ, enhancing their functionality and shifting them toward a pro-inflammatory phenotype by increasing the $M1_{(iNOS)}$-to-$M2_{(ARG1)}$ ratio. UVB also induced metabolic adjustments, including downregulation of 1α-hydroxylase, catalase activity, and $_{tcc}$CHOL—a well-established signature of trained immunity. Notably, UVB exposure led to a marked increase in MPO activity—indicative of METosis-like oxidative responses in PRMφs, but this effect was significantly reversed by the simulated physical barrier (rat fur), with MPO levels returning close to baseline. This underscores MPO's dual role in inflammation: while it aids host defense by producing reactive oxidants—most notably HOCl, a potent antimicrobial—it can also cause collateral tissue damage when excessively or chronically activated. Attenuating MPO activity may therefore help reduce oxidative stress and limit inflammation; by contrast, broad or unregulated inhibition without protective mechanisms could compromise immune competence. These

findings highlight the need for a targeted, context-aware approach to MPO modulation—one that maximizes therapeutic benefit while minimizing unintended harm.

These findings emphasize PRMφ's role in extrarenal vitamin D metabolism and support the concept of tissue-resident macrophages serving as local "active reservoirs" of vitamin D. This non-circulating form of vitamin D, likely produced under UVB influence, could be directly utilized by immune cells to modulate localized immune responses. Our results highlight the need to go beyond circulating 25-hydroxyvitamin D levels as the sole indicator of vitamin D status and to consider tissue-specific dynamics, particularly in contexts where compensatory mechanisms are likely to influence vitamin D metabolism and utilization.

Future studies should focus on the role of tissue-resident macrophages as local vitamin D reservoirs, the long-term impact of UVB exposure on macrophage function, and the influence of passive physical barriers such as fabric or other UV-blocking materials. Additionally, extending these findings to disease models may uncover therapeutic opportunities for modulating macrophage function and vitamin D metabolism in immune-related conditions. Moreover, circadian rhythms should not be overlooked, as they can influence both macrophage reactivity and UVB-induced signaling. Incorporating temporal aspects into future experimental designs may offer deeper insights into the dynamics of immune modulation under photobiological conditions.

Beyond the insights gained from macrophage-specific effects, it is also necessary to consider the broader cellular context within which these interactions take place. Therefore, although our study centered on macrophage responses, it is important to recognize that UVB radiation and vitamin D signaling likely exert effects on multiple cell populations within the tissue microenvironment. In particular, epithelial and stromal cells are known to contribute to local immune regulation and may respond differentially to photobiological stimuli. Future studies should also investigate how these findings in a preclinical rat model could be translated to human health, with a particular focus on additional cell types involved in UVB- and vitamin D-mediated immune modulation.

Data availability statement

The original contributions presented in the study are included in the article/supplementary material. Further inquiries can be directed to the corresponding authors.

Ethics statement

The study was conducted in compliance with Good Laboratory Practices (GLP) and approved by the Faculty Scientific Council/Institutional Ethics Committee of Tlemcen University. Measures were implemented to prevent and alleviate any potential pain or distress, in alignment with ethical principles that emphasize minimizing animal suffering whenever feasible, while ensuring the scientific justification of procedures (180).

Author contributions

FSM: Writing – original draft, Writing – review & editing, Data curation, Investigation, Methodology. SZ: Writing – review & editing, Data curation, Investigation, Methodology. NEB: Writing – review & editing, Data curation, Investigation, Methodology. RM: Writing – review & editing, Data curation, Investigation, Methodology. FB: Data curation, Investigation, Methodology, Writing – review & editing. CE: Formal analysis, Investigation, Methodology, Writing – review & editing. NBN: Formal analysis, Writing – review & editing. ZM: Formal analysis, Investigation, Methodology, Writing – review & editing. SB: Formal analysis, Investigation, Methodology, Writing – review & editing. FJDM: Writing – review & editing, Resources. CT: Writing – review & editing, Resources. XL: Conceptualization, Writing – review & editing, Supervision, Resources. AB: Conceptualization, Writing – review & editing, Supervision, Resources. MA: Writing – original draft, Conceptualization, Writing – review & editing, Supervision, Methodology, Formal analysis, Resources.

Funding

The author(s) declare financial support was received for the research and/or publication of this article. This research was conducted with partial support from the Laboratory of Applied Molecular Biology and Immunology (W0414100, University of Tlemcen, Algeria), under the Directorate General of Scientific Research and Technological Development (DGRSDT, MESRS, Algeria).

Acknowledgments

The authors are deeply grateful to the Immunity teams of the Laboratory of Applied Molecular Biology and Immunology for their technical assistance. They also sincerely thank MSc Taleb Aridj, MSc Houria benarraddj, MSc Zakariya Bensefeia, MSc Hicham Zerrouk for their intellectual and technical support.

Conflict of interest

The authors declare that the research was conducted in the absence of any commercial or financial relationships that could be construed as a potential conflict of interest.

Generative AI statement

The author(s) declare that Generative AI was used in the creation of this manuscript, exclusively to enhance English language editing. The authors thoroughly reviewed all AI-assisted content to ensure its accuracy and relevance to the study.

Publisher's note

References

1. Carmeliet G, Dermauw V, Bouillon R. Vitamin D signaling in calcium and bone homeostasis: A delicate balance. *Best Pract Res Clin Endocrinol Metab*. (2015) 29:621–31. doi: 10.1016/j.beem.2015.06.001

2. Janoušek J, Pilařová V, Macáková K, Nomura A, Veiga-Matos J, Silva DDD, et al. Vitamin D: sources, physiological role, biokinetics, deficiency, therapeutic use, toxicity, and overview of analytical methods for detection of vitamin D and its metabolites. *Crit Rev Clin Lab Sci*. (2022) 59(8):517–54. doi: 10.1080/10408363.2022.2070595

3. Aribi M, Mennechet FJD, Touil-Boukoffa C. Editorial: The role of vitamin D as an immunomodulator. *Front Immunol*. (2023) 14:1186635. doi: 10.3389/fimmu.2023.1186635

4. Nouari W, Ysmail-Dahlouk L, Aribi M. Vitamin D3 enhances bactericidal activity of macrophage against Pseudomonas aeruginosa. *Int Immunopharmacol*. (2016) 30:94–101. doi: 10.1016/j.intimp.2015.11.033

5. Chun RF, Shieh A, Gottlieb C, Yacoubian V, Wang J, Hewison M, et al. Vitamin D binding protein and the biological activity of vitamin D. *Front Endocrinol*. (2019) 10:718. doi: 10.3389/fendo.2019.00718

6. Lopez DV, Al-Jaberi FAH, Woetmann A, Ødum N, Bonefeld CM, Kongsbak-Wismann M, et al. Macrophages control the bioavailability of vitamin D and vitamin D-regulated T cell responses. *Front Immunol*. (2021) 12:722806. doi: 10.3389/fimmu.2021.722806

7. Yousefzadeh P, Shapses SA, Wang X. Vitamin D binding protein impact on 25-hydroxyvitamin D levels under different physiologic and pathologic conditions. *Int J Endocrinol*. (2014) 2014:981581. doi: 10.1155/2014/981581

8. Rowling MJ, Kemmis CM, Taffany DA, Welsh J. Megalin-mediated endocytosis of vitamin D binding protein correlates with 25-hydroxycholecalciferol actions in human mammary cells. *J Nutr*. (2006) 136:2754–9. doi: 10.1093/jn/136.11.2754

9. Nykjaer A, Fyfe JC, Kozyraki R, Leheste JR, Jacobsen C, Nielsen MS, et al. Cubilin dysfunction causes abnormal metabolism of the steroid hormone 25(OH) vitamin D (3). *Proc Natl Acad Sci U S A*. (2001) 98:13895–900. doi: 10.1073/pnas.241516998

10. Ao T, Kikuta J, Ishii M. The effects of vitamin D on immune system and inflammatory diseases. *Biomolecules*. (2021) 11:1624. doi: 10.3390/biom11111624

11. Marwaha RK, Sreenivas V, Talwar D, Yenamandra VK, Challa A, Lakshmy R, et al. Impact of solar ultraviolet B radiation (290–320 nm) on vitamin D synthesis in children with type IV and V skin. *Br J Dermatol*. (2015) 173:604–6. doi: 10.1111/bjd.13887

12. O'Neill C, Kazantzidis A, Ryan M, Barber N, Sempos C, Durazo-Arvizu R, et al. Seasonal changes in vitamin D-effective UVB availability in Europe and associations with population serum 25-hydroxyvitamin D. *Nutrients*. (2016) 8:533. doi: 10.3390/nu8090533

13. Fajuyigbe D, Lwin SM, Diffey BL, Baker R, Tobin DJ, Sarkany RPE, et al. Melanin distribution in human epidermis affords localized protection against DNA photodamage and concurs with skin cancer incidence difference in extreme phototypes. *FASEB J*. (2018) 32:3700–6. doi: 10.1096/fj.201701472R

14. Tsiaras W, Weinstock M. Factors influencing vitamin D status. *Acta Derm Venerol*. (2011) 91:115–24. doi: 10.2340/00015555-0980

15. Passeron T, Bouillon R, Callender V, Cestari T, Diepgen TL, Green AC, et al. Sunscreen photoprotection and vitamin D status. *Br J Dermatol*. (2019) 181:916–31. doi: 10.1111/bjd.17992

16. Lips P, van Schoor NM, de Jongh RT. Diet, sun, and lifestyle as determinants of vitamin D status. *Ann NY Acad Sci*. (2014) 1317:92–8. doi: 10.1111/nyas.12443

17. Berry EG, Bezecny J, Acton M, Sulmonetti TP, Anderson DM, Beckham HW, et al. Slip versus slop: A head-to-head comparison of UV-protective clothing to sunscreen. *Cancers*. (2022) 14:542. doi: 10.3390/cancers14030542

18. Neville JJ, Palmieri T, Young AR. Physical determinants of vitamin D photosynthesis: A review. *JBMR Plus*. (2021) 5(1):e10460. doi: 10.1002/jbm4.10460

19. Lee M-S, Bensinger SJ. Reprogramming cholesterol metabolism in macrophages and its role in host defense against cholesterol-dependent cytolysins. *Cell Mol Immunol*. (2022) 19:327–36. doi: 10.1038/s41423-021-00827-0

20. Christakos S, Dhawan P, Verstuyf A, Verlinden L, Carmeliet G. Vitamin D: metabolism, molecular mechanism of action, and pleiotropic effects. *Physiol Rev*. (2016) 96:365–408. doi: 10.1152/physrev.00014.2015

21. Shany S, Rapoport J, Zuili I, Gavriel A, Lavi N, Chaimovitz C. Metabolism of 25-OH-vitamin D3 by peritoneal macrophages from CAPD patients. *Kidney Int*. (1991) 39:1005–11. doi: 10.1038/ki.1991.127

22. De Jesus A, Pusec CM, Nguyen T, Keyhani-Nejad F, Gao P, Weinberg SE, et al. Optimized protocol to isolate primary mouse peritoneal macrophage metabolites. *STAR Protoc*. (2022) 3:101668. doi: 10.1016/j.xpro.2022.101668

23. Song L, Papaioannou G, Zhao H, Luderer HF, Miller C, Dall'Osso C, et al. The vitamin D receptor regulates tissue resident macrophage response to injury. *Endocrinology*. (2016) 157:4066–75. doi: 10.1210/en.2016-1474

24. Rehermann B. Mature peritoneal macrophages take an avascular route into the injured liver and promote tissue repair. *Hepatology*. (2017) 65:376–9. doi: 10.1002/hep.28883

25. García-Peñarrubia P, Ruiz-Alcaraz AJ, Ruiz-Ballester M, Ramírez-Pávez TN, Martínez-Esparza M. Recent insights into the characteristics and role of peritoneal macrophages from ascites of cirrhotic patients. *World J Gastroenterol*. (2021) 27:7014–24. doi: 10.3748/wjg.v27.i41.7014

26. Ardavín C, Alvarez-Ladrón N, Ferriz M, Gutiérrez-González A, Vega-Pérez A. Mouse tissue-resident peritoneal macrophages in homeostasis, repair, infection, and tumor metastasis. *Adv Sci (Weinh)*. (2023) 10:e2206617. doi: 10.1002/advs.202206617

27. Liu T, Liu F, Peng L-W, Chang L, Jiang Y-M. The peritoneal macrophages in inflammatory diseases and abdominal cancers. *Oncol Res*. (2018) 26:817–26. doi: 10.3727/096504017X15130753659625

28. Hu K, Scheer FAJL, Buijs RM, Shea SA. The circadian pacemaker generates similar circadian rhythms in the fractal structure of heart rate in humans and rats. *Cardiovasc Res*. (2008) 80:62–8. doi: 10.1093/cvr/cvn150

29. Shirato K, Sato S. Macrophage meets the circadian clock: implication of the circadian clock in the role of macrophages in acute lower respiratory tract infection. *Front Cell Infect Microbiol*. (2022) 12:826738. doi: 10.3389/fcimb.2022.826738

30. Keller M, Mazuch J, Abraham U, Eom GD, Herzog ED, Volk H-D, et al. A circadian clock in macrophages controls inflammatory immune responses. *Proc Natl Acad Sci U.S.A*. (2009) 106:21407–12. doi: 10.1073/pnas.0906361106

31. Fukuta K. Collection of body fluids. In: *The Laboratory Mouse*. Amsterdam, Netherlands: Elsevier (2012). p. 727–38. doi: 10.1016/B978-0-12-382008-2.00031-3

32. Dai JH, Iwatani Y, Ishida T, Terunuma H, Kasai H, Iwakula Y, et al. Glycyrrhizin enhances interleukin-12 production in peritoneal macrophages. *Immunology*. (2001) 103:235–43. doi: 10.1046/j.1365-2567.2001.01224.x

33. Aribi M, Meziane W, Habi S, Boulatika Y, Marchandin H, Aymeric J-L. Macrophage Bactericidal Activities against Staphylococcus aureus Are Enhanced *In Vivo* by Selenium Supplementation in a Dose-Dependent Manner. *PLoS One*. (2015) 10:e0135515. doi: 10.1371/journal.pone.0135515

34. Lu R, Sampathkumar NK, Benayoun BA. Measuring phagocytosis in bone marrow-derived macrophages and peritoneal macrophages with aging. *Methods Mol Biol*. (2020) 2144:161–70. doi: 10.1007/978-1-0716-0592-9_14

35. Okerblom JJ, Schwarz F, Olson J, Fletes W, Ali SR, Martin PT, et al. Loss of CMAH during Human Evolution Primed the Monocyte-Macrophage Lineage toward a More Inflammatory and Phagocytic State. *J Immunol*. (2017) 198:2366–73. doi: 10.4049/jimmunol.1601471

36. Piccinini F, Tesei A, Arienti C, Bevilacqua A. Cell counting and viability assessment of 2D and 3D cell cultures: expected reliability of the trypan blue assay. *Biol Proced Online*. (2017) 19:8. doi: 10.1186/s12575-017-0056-3

37. Kift RC, Webb AR. Globally estimated UVB exposure times required to maintain sufficiency in vitamin D levels. *Nutrients*. (2024) 16:1489. doi: 10.3390/nu16101489

38. Aguilera J, Navarrete-de Gálvez E, Sánchez-Roldán C, Herrera-Ceballos E, de Gálvez MV. Sun-protective properties of technical sportswear fabrics 100% Polyester: the influence of moisture and sweat on protection against different biological effects of ultraviolet (UV) radiation. *Photochem Photobiol*. (2023) 99:184–92. doi: 10.1111/php.13679

39. Park K, Frey MW. Designing an effective and scalable UV-protective cooling textile with nanoporous fibers. *Nano Lett*. (2023) 23:10398–405. doi: 10.1021/acs.nanolett.3c03055

40. Aguilera J, de Gálvez MV, Sánchez-Roldán C, Herrera-Ceballos E. New advances in protection against solar ultraviolet radiation in textiles for summer clothing. *Photochem Photobiol*. (2014) 90:1199–206. doi: 10.1111/php.12292

41. Gambichler T, Laperre J, Hoffmann K. The European standard for sun-protective clothing: EN 13758. *J Eur Acad Dermatol Venereol*. (2006) 20:125–30. doi: 10.1111/j.1468-3083.2006.01401.x

42. Gambichler T, Rotterdam S, Altmeyer P, Hoffmann K. Protection against ultraviolet radiation by commercial summer clothing: need for standardised testing and labelling. *BMC Dermatol.* (2001) 1:6. doi: 10.1186/1471-5945-1-6

43. Khvatov IA, Ganza PN, Kharitonov AN, Samuleeva MV. Wistar Male Rats (Rattus norvegicus domestica) Are Aware of Their Dimensions. *Animals.* (2024) 14:3384. doi: 10.3390/ani14233384

44. Peña-Escudero C, Priego-Fernández S, Caba M, Rodríguez-Alba JC, Corona-Morales AA, García-García F. Effect of a hedonic stimulus on the sleep architecture of male wistar rats. *Sleep Sci.* (2023) 16:e329–34. doi: 10.1055/s-0043-1773788

45. de Gálvez MV, Aguilera J, Bernabó J-L, Sánchez-Roldán C, Herrera-Ceballos E. Human hair as a natural sun protection agent: A quantitative study. *Photochem Photobiol.* (2015) 91:966–70. doi: 10.1111/php.12433

46. Miliani M, Nouar M, Paris O, Lefranc G, Mennechet F, Aribi M. Thymoquinone potently enhances the activities of classically activated macrophages pulsed with necrotic jurkat cell lysates and the production of antitumor Th1-/M1-related cytokines. *J Interferon Cytokine Res.* (2018) 38:539–51. doi: 10.1089/jir.2018.0010

47. Bisswanger H. Enzyme assays. *Perspect Sci.* (2014) 1:41–55. doi: 10.1016/j.pisc.2014.02.005

48. Smith AF, Taylor RH. Comparison of two-point (AutoAnalyzer II) with kinetic methods for transaminase assay. *J Clin Pathol.* (1973) 26:42–7. doi: 10.1136/jcp.26.1.42

49. Chauhan AK, Jakhar R, Paul S, Kang SC. Potentiation of macrophage activity by thymol through augmenting phagocytosis. *Int Immunopharmacol.* (2014) 18:340–6. doi: 10.1016/j.intimp.2013.11.025

50. Segal AW. Nitroblue-tetrazolium tests. *Lancet.* (1974) 2:1248–52. doi: 10.1016/s0140-6736(74)90758-2

51. Sim Choi H, Woo Kim J, Cha Y, Kim C. A quantitative nitroblue tetrazolium assay for determining intracellular superoxide anion production in phagocytic cells. *J Immunoassay Immunochemistry.* (2006) 27:31–44. doi: 10.1080/15321810500403722

52. Aribi M. Macrophage bactericidal assays. In: Rousselet G, editor. *Macrophages. Methods in Molecular Biology.* Springer New York, New York, NY (2018). p. 135–49. doi: 10.1007/978-1-4939-7837-3_14

53. Thomas DC. The phagocyte respiratory burst: Historical perspectives and recent advances. *Immunol Lett.* (2017) 192:88–96. doi: 10.1016/j.imlet.2017.08.016

54. Meziane W, Mekkaoui Z, Hai I, Kacimi K, Djilali K, Touil-Boukoffa C, et al. Combination of metformin with sodium selenite induces a functional phenotypic switch of human GM-CSF monocyte-derived macrophages. *Int Immunopharmacol.* (2019) 73:212–24. doi: 10.1016/j.intimp.2019.05.004

55. Kumar K, Margerum DW. Kinetics and mechanism of general-acid-assisted oxidation of bromide by hypochlorite and hypochlorous acid. *Inorg Chem.* (1987) 26:2706–11. doi: 10.1021/ic00263a030

56. Harwood DT, Kettle AJ, Winterbourn CC. Production of glutathione sulfonamide and dehydroglutathione from GSH by myeloperoxidase-derived oxidants and detection using a novel LC-MS/MS method. *Biochem J.* (2006) 399:161–8. doi: 10.1042/BJ20060978

57. Waters JW, Froidevaux L, Harwood RS, Jarnot RF, Pickett HM, Read WG, et al. The Earth observing system microwave limb sounder (EOS MLS) on the aura Satellite. *IEEE Trans Geosci Remote Sens.* (2006) 44:1075–92. doi: 10.1109/TGRS.2006.873771

58. Pulli B, Ali M, Forghani R, Schob S, Hsieh KLC, Wojtkiewicz G, et al. Measuring myeloperoxidase activity in biological samples. *PloS One.* (2013) 8:e67976. doi: 10.1371/journal.pone.0067976

59. Farcas MT, Kisin ER, Menas AL, Gutkin DW, Star A, Reiner RS, et al. Pulmonary exposure to cellulose nanocrystals caused deleterious effects to reproductive system in male mice. *J Toxicol Environ Health A.* (2016) 79:984–97. doi: 10.1080/15287394.2016.1211045

60. Mills CD. M1 and M2 macrophages: oracles of health and disease. *Crit Rev Immunol.* (2012) 32:463–88. doi: 10.1615/critrevimmunol.v32.i6.10

61. Rath M, Müller I, Kropf P, Closs EI, Munder M. Metabolism via arginase or nitric oxide synthase: two competing arginine pathways in macrophages. *Front Immunol.* (2014) 5:532. doi: 10.3389/fimmu.2014.00532

62. Nouar M, Miliani M, Belhassena I, Fatmi A, Aribi M. Sodium selenite modulates global activation of proinflammatory M1-like macrophages, necroinflammation and M1-like/M2-like dichotomy at the onset of human type 1 diabetes. *Endocr Metab Immune Disord Drug Targets.* (2023) 23:1104–17. doi: 10.2174/1871530323666230201135916

63. Dahou S, Smahi MC-E, Nouari W, Dahmani Z, Benmansour S, Ysmail-Dahlouk L, et al. L-Threoascorbic acid treatment promotes S. aureus-infected primary human endothelial cells survival and function, as well as intracellular bacterial killing, and immunomodulates the release of IL-1β and soluble ICAM-1. *Int Immunopharmacol.* (2021) 95:107476. doi: 10.1016/j.intimp.2021.107476

64. Aribi M. Macrophage bactericidal assays. *Methods Mol Biol.* (2018) 1784:135–49. doi: 10.1007/978-1-4939-7837-3_14

65. Barham D, Trinder P. An improved colour reagent for the determination of blood glucose by the oxidase system. *Analyst.* (1972) 97:142–5. doi: 10.1039/an9729700142

66. McBurney RN, Neering IR. The measurement of changes in intracellular free calcium during action potentials in mammalian neurones. *J Neurosci Methods.* (1985) 13:65–76. doi: 10.1016/0165-0270(85)90044-5

67. Chutipongtanate S, Thongboonkerd V. Establishment of a novel colorimetric assay for high-throughput analysis of calcium oxalate crystal growth modulation. *Analyst.* (2010) 135:1309–14. doi: 10.1039/B927046A

68. Dwivedi AK, Mallawaarachchi I, Alvarado LA. Analysis of small sample size studies using nonparametric bootstrap test with pooled resampling method. *Stat Med.* (2017) 36:2187–205. doi: 10.1002/sim.7263

69. Taylor PR, Gordon S. Monocyte heterogeneity and innate immunity. *Immunity.* (2003) 19:2–4. doi: 10.1016/S1074-7613(03)00178-X

70. Gordon S. The macrophage: Past, present and future. *Eur J Immunol.* (2007) 37: S9–S17. doi: 10.1002/eji.200737638

71. Wynn TA, Chawla A, Pollard JW. Macrophage biology in development, homeostasis and disease. *Nature.* (2013) 496:445–55. doi: 10.1038/nature12034

72. Cassado ADA, D'Império Lima MR, Bortoluci KR. Revisiting mouse peritoneal macrophages: heterogeneity, development, and function. *Front Immunol.* (2015) 6:225. doi: 10.3389/fimmu.2015.00225

73. Murray HW, Spitalny GL, Nathan CF. Activation of mouse peritoneal macrophages *in vitro* and *in vivo* by interferon-gamma. *J Immunol.* (1985) 134:1619–22. doi: 10.4049/jimmunol.134.3.1619

74. Hayashi M, Shimba S, Tezuka M. Characterization of the molecular clock in mouse peritoneal macrophages. *Biol Pharm Bull.* (2007) 30:621–6. doi: 10.1248/bpb.30.621

75. Gurusmatika S, Ishida M, Nishi K, Sugahara T. Exploring the anti-inflammatory effect of clove water extract in lipopolysaccharide-stimulated RAW264.7 cells and mouse peritoneal macrophages. *J Food Bioactives.* (2024) 25:72–80. doi: 10.31665/JFB.2024.18373

76. Balog S, Jeong S, Asahina K. Recruitment of large peritoneal macrophages to capsular fibrosis developed on the liver surface. *FASEB J.* (2024) 38:e23327. doi: 10.1096/fj.202301187R

77. Ullrich SE, Kripke ML, Ananthaswamy HN. Mechanisms underlying UV-induced immune suppression: implications for sunscreen design. *Exp Dermatol.* (2002) 11:13–6. doi: 10.1034/j.1600-0625.11.s.1.4.x

78. Slominski RM, Chen JY, Raman C, Slominski AT. Photo-neuro-immuno-endocrinology: How the ultraviolet radiation regulates the body, brain, and immune system. *Proc Natl Acad Sci U S A.* (2024) 121:e2308374121. doi: 10.1073/pnas.2308374121

79. Yu Z, Zheng M, Fan H, Liang X, Tang Y. Ultraviolet (UV) radiation: a double-edged sword in cancer development and therapy. *Mol BioMed.* (2024) 5:49. doi: 10.1186/s43556-024-00209-8

80. Oshina I, Spigulis J. Beer-Lambert law for optical tissue diagnostics: current state of the art and the main limitations. *J BioMed Opt.* (2021) 26:100901. doi: 10.1117/1.JBO.26.10.100901

81. Baranoski GVG, Krishnaswamy A. *Light & skin interactions: simulations for computer graphics applications.* Amsterdam: Morgan Kaufmann (2010).

82. Kostyuk V, Potapovich A, Albuhaydar AR, Mayer W, De Luca C, Korkina L. Natural substances for prevention of skin photoaging: screening systems in the development of sunscreen and rejuvenation cosmetics. *Rejuvenation Res.* (2018) 21:91–101. doi: 10.1089/rej.2017.1931

83. Hawk JLM. Safe, mild ultraviolet-B exposure: An essential human requirement for vitamin D and other vital bodily parameter adequacy: A review. *Photodermatol Photoimmunol Photomed.* (2020) 36:417–23. doi: 10.1111/phpp.12584

84. Norval M, Lucas RM, Cullen AP, de Gruijl FR, Longstreth J, Takizawa Y, et al. The human health effects of ozone depletion and interactions with climate change. *Photochem Photobiol Sci.* (2011) 10:199–225. doi: 10.1039/c0pp90044c

85. Fletcher J, Bishop EL, Harrison SR, Swift A, Cooper SC, Dimeloe SK, et al. Autoimmune disease and interconnections with vitamin D. *Endocr Connect.* (2022) 11: e210554. doi: 10.1530/EC-21-0554

86. Sieminska I, Pieniawska M, Grzywa TM. The immunology of psoriasis-current concepts in pathogenesis. *Clin Rev Allergy Immunol.* (2024) 66:164–91. doi: 10.1007/s12016-024-08991-7

87. Sajja AP, Joshi AA, Teague HL, Dey AK, Mehta NN. Potential immunological links between psoriasis and cardiovascular disease. *Front Immunol.* (2018) 9:1234. doi: 10.3389/fimmu.2018.01234

88. Clark RA, Kupper TS. Misbehaving macrophages in the pathogenesis of psoriasis. *J Clin Invest.* (2006) 116:2084–7. doi: 10.1172/JCI29441

89. Liu S-H, Zhang J, Zuo Y-G. Macrophages in inflammatory skin diseases and skin tumors. *Front Immunol.* (2024) 15:1430825. doi: 10.3389/fimmu.2024.1430825

90. Kasraie S, Werfel T. Role of macrophages in the pathogenesis of atopic dermatitis. *Mediators Inflammation.* (2013) 2013:942375. doi: 10.1155/2013/942375

91. Tian XQ, Holick MF. Catalyzed thermal isomerization between previtamin D3 and vitamin D3 via β-cyclodextrin complexation. *J Biol Chem.* (1995) 270:8706–11. doi: 10.1074/jbc.270.15.8706

92. Delrue C, Speeckaert MM. Vitamin D and vitamin D-binding protein in health and disease. *IJMS.* (2023) 24:4642. doi: 10.3390/ijms24054642

93. Masood T, Kushwaha RS, Singh R, Sailwal S, Pandey H, Varma A, et al. Circadian rhythm of serum 25 (OH) vitamin D, calcium and phosphorus levels in

the treatment and management of type-2 diabetic patients. *DD&T*. (2015) 9:70–4. doi: 10.5582/ddt.2015.01002

94. Stephenson A, Mamo JCL, Takechi R, Hackett MJ, Lam V. Genetic, environmental and biomarker considerations delineating the regulatory effects of vitamin D on central nervous system function. *Br J Nutr*. (2020) 123:41–58. doi: 10.1017/S000711451900268X

95. Romano F, Muscogiuri G, Di Benedetto E, Zhukouskaya VV, Barrea L, Savastano S, et al. Vitamin D and sleep regulation: is there a role for vitamin D? *CPD*. (2020) 26:2492–6. doi: 10.2174/1381612826666200310145935

96. Huiberts LM, Smolders KCHJ. Effects of vitamin D on mood and sleep in the healthy population: Interpretations from the serotonergic pathway. *Sleep Med Rev*. (2021) 55:101379. doi: 10.1016/j.smrv.2020.101379

97. Prono F, Bernardi K, Ferri R, Bruni O. The role of vitamin D in sleep disorders of children and adolescents: A systematic review. *IJMS*. (2022) 23:1430. doi: 10.3390/ijms23031430

98. Jeevan A, Bucana CD, Dong Z, Dizon VV, Thomas SL, Lloyd TE, et al. Ultraviolet radiation reduces phagocytosis and intracellular killing of mycobacteria and inhibits nitric oxide production by macrophages in mice. *J Leukocyte Biol*. (1995) 57:883–90. doi: 10.1002/jlb.57.6.883

99. Kasahara S, Aizawa K, Okamiya M, Kazuno N, Mutoh S, Fugo H, et al. Uvb irradiation suppresses cytokine production and innate cellular immune functions in mice. *Cytokine*. (2001) 14:104–11. doi: 10.1006/cyto.2001.0849

100. Sethi G, Sodhi A. *In vitro* activation of murine peritoneal macrophages by ultraviolet B radiation: upregulation of CD18, production of NO, proinflammatory cytokines and a signal transduction pathway. *Mol Immunol*. (2004) 40:1315–23. doi: 10.1016/j.molimm.2004.01.001

101. Vaccaro M, Irrera N, Cutroneo G, Rizzo G, Vaccaro F, Anastasi G, et al. Differential Expression of Nitric Oxide Synthase Isoforms nNOS and iNOS in Patients with Non-Segmental Generalized Vitiligo. *IJMS*. (2017) 18:2533. doi: 10.3390/ijms18122533

102. Sur R, Heck DE, Mariano TM, Jin Y, Murphy WJ, Laskin JD. UVB light suppresses nitric oxide production by murine keratinocytes and macrophages. *Biochem Pharmacol*. (2002) 64:1469–81. doi: 10.1016/S0006-2952(02)01419-3

103. Inaba I, Hiramoto K, Yamate Y, Morita A, Tsutsumi T, Yasuda H, et al. Inhibiting neutrophil extracellular traps protects against ultraviolet B-induced skin damage: effects of Hochu-ekki-to and DNase I. *Int J Mol Sci*. (2024) 25:1723. doi: 10.3390/ijms25031723

104. Zhou X, Du H-H, Long X, Pan Y, Hu J, Yu J, et al. β-Nicotinamide mononucleotide (NMN) administrated by intraperitoneal injection mediates protection against UVB-induced skin damage in mice. *JIR*. (2021) 14:5165–82. doi: 10.2147/JIR.S327329

105. Xue S, Zang Y, Chen J, Shang S, Gao L, Tang X. Ultraviolet-B radiation stress triggers reactive oxygen species and regulates the antioxidant defense and photosynthesis systems of intertidal red algae Neoporphyra haitanensis. *Front Mar Sci*. (2022) 9:1043462. doi: 10.3389/fmars.2022.1043462

106. Luther CA, Lim HW. Solar Angioedema: A report of a patient and a review of literature. *Photoderm Photoimm Photomed*. (2019) 35:187–9. doi: 10.1111/phpp.12445

107. Fan J, Watanabe T. Atherosclerosis: known and unknown. *Pathol Int*. (2022) 72:151–60. doi: 10.1111/pin.13202

108. Falk E. Pathogenesis of atherosclerosis. *J Am Coll Cardiol*. (2006) 47:C7–C12. doi: 10.1016/j.jacc.2005.09.068

109. Heinecke JW. Oxidative stress: new approaches to diagnosis and prognosis in atherosclerosis. *Am J Cardiol*. (2003) 91:12–6. doi: 10.1016/S0002-9149(02)03145-4

110. McMillen TS, Heinecke JW, LeBoeuf RC. Expression of human myeloperoxidase by macrophages promotes atherosclerosis in mice. *Circulation*. (2005) 111:2798–804. doi: 10.1161/CIRCULATIONAHA.104.516278

111. Sugiyama S, Okada Y, Sukhova GK, Virmani R, Heinecke JW, Libby P. Macrophage myeloperoxidase regulation by granulocyte macrophage colony-stimulating factor in human atherosclerosis and implications in acute coronary syndromes. *Am J Pathol*. (2001) 158:879–91. doi: 10.1016/S0002-9440(10)64036-9

112. Veauthier B, Hornecker JR. Crohn's disease: diagnosis and management. *Am Fam Physician*. (2018) 98:661–9.

113. Ballester Ferré MP, Boscá-Watts MM, Mínguez Pérez M. Enfermedad de crohn. *Medicina Clínica*. (2018) 151:26–33. doi: 10.1016/j.medcli.2017.10.036

114. Liu Y, Liu L. The pro-tumor effect and the anti-tumor effect of neutrophils extracellular traps. *BST*. (2019) 13:469–75. doi: 10.5582/bst.2019.01326

115. Ali M, Fulci G, Grigalavicius M, Pulli B, Li A, Wojtkiewicz GR, et al. Myeloperoxidase exerts anti-tumor activity in glioma after radiotherapy. *Neoplasia*. (2022) 26:100779. doi: 10.1016/j.neo.2022.100779

116. Islam M, Akter T, Ferdush J, Kamrunnahar K. Impact of fabric density, color and composition of plain weave fabric on ultraviolet protective factor. *GJRE*. (2019) 19:13–5. doi: 10.34257/GJREJVOL19IS1PG13

117. Saravanan D. Uv protection textile materials. *AUTEX Res J*. (2007) 7:53–62. doi: 10.1515/aut-2007-070106

118. Rahman N, Dafader NC. Radiation technology for the modification of textiles. In: *Fundamentals of Natural Fibres and Textiles*. Amsterdam, Netherlands: Elsevier (2021). p. 407–38. doi: 10.1016/B978-0-12-821483-1.00003-6

119. Davis S, Capjack L, Kerr N, Fedosejcvs R. Clothing as protection from ultraviolet radiation: which fabric is most effective? *Int J Dermatol*. (1997) 36:374–9. doi: 10.1046/j.1365-4362.1997.00046.x

120. Khan A, Nazir A, Rehman A, Naveed M, Ashraf M, Iqbal K, et al. A review of UV radiation protection on humans by textiles and clothing. *IJCST*. (2020) 32:869–90. doi: 10.1108/IJCST-10-2019-0153

121. Koti RS, Tsui JC, Lobos E, Yang W, Seifalian AM, Davidson BR. Nitric oxide synthase distribution and expression with ischemic preconditioning of the rat liver. *FASEB J*. (2005) 19:1155–7. doi: 10.1096/fj.04-3220fje

122. Hu X, Li Y, Cao Y, Shi F, Shang L. The role of nitric oxide synthase/nitric oxide in infection-related cancers: Beyond antimicrobial activity. *Biochim Biophys Acta (BBA) - Rev Cancer*. (2024) 1879:189156. doi: 10.1016/j.bbcan.2024.189156

123. Dzik JM. Evolutionary roots of arginase expression and regulation. *Front Immunol*. (2014) 5:544. doi: 10.3389/fimmu.2014.00544

124. Orecchioni M, Ghosheh Y, Pramod AB, Ley K. Macrophage Polarization: Different Gene Signatures in M1(LPS+) vs. Classically and M2(LPS–) vs. Alternatively Activated Macrophages. *Front Immunol*. (2019) 10:1084. doi: 10.3389/fimmu.2019.01084

125. Lee KY. M1 and M2 polarization of macrophages: a mini-review. *Med Biol Sci Eng*. (2019) 2:1–5. doi: 10.30579/mbse.2019.2.1.1

126. Abbas S, Alam S, Pal A, Kumar M, Singh D, Ansari KM. UVB exposure enhanced benzanthrone-induced inflammatory responses in SKH-1 mouse skin by activating the expression of COX-2 and iNOS through MAP kinases/NF-κB/AP-1 signalling pathways. *Food Chem Toxicol*. (2016) 96:183–90. doi: 10.1016/j.fct.2016.07.034

127. Kuhn A, Fehsel K, Lehmann P, Krutmann J, Ruzicka T, Kolb-Bachofen V. Aberrant timing in epidermal expression of inducible nitric oxide synthase after UV irradiation in cutaneous lupus erythematosus. *J Invest Dermatol*. (1998) 111:149–53. doi: 10.1046/j.1523-1747.1998.00253.x

128. Chang H-R, Tsao D-A, Wang S-R, Yu H-S. Expression of nitric oxide synthases in keratinocytes after UVB irradiation. *Arch Dermatol Res*. (2003) 295:293–6. doi: 10.1007/s00403-003-0433-4

129. Park G, Cui Y, Yang S, Sun M, Wilkinson E, Li H, et al. Moderate low UVB irradiation modulates tumor-associated macrophages and dendritic cells and promotes antitumor immunity in tumor-bearing mice†. *Photochem Photobiol*. (2023) 99:850–6. doi: 10.1111/php.13684

130. Hafeez BB, Alvarado EW, Kim DJ. Therapeutic implications of UVB irradiation in cancer by enhancing anti-tumor immunity†. *Photochem Photobiol*. (2023) 99:874–7. doi: 10.1111/php.13729

131. Karisola P, Nikkola V, Joronen H, Ylianttila L, Grönroos M, Partonen T, et al. Narrow-band UVB radiation triggers diverse changes in the gene expression and induces the accumulation of M1 macrophages in human skin. *J Photochem Photobiol B: Biol*. (2024) 253:112887. doi: 10.1016/j.jphotobiol.2024.112887

132. Liu T, Zhang L, Joo D, Sun S-C. NF-κB signaling in inflammation. *Sig Transduct Target Ther*. (2017) 2:17023. doi: 10.1038/sigtrans.2017.23

133. Bi Z. Increased MAPK. and NF-κB expression of Langerhans cells is dependent on TLR2 and TLR4, and increased IRF-3 expression is partially dependent on TLR4 following UV exposure. *Mol Med Rep*. (2011) 4:541–6. doi: 10.3892/mmr.2011.450

134. Park G, Qian W, Zhang M-J, Chen Y-H, Ma L-W, Zeng N, et al. Platelet-rich plasma regulating the repair of ultraviolet B–induced acute tissue inflammation: adjusting macrophage polarization through the activin receptor–follistatin system. *Bioengineered*. (2021) 12:3125–36. doi: 10.1080/21655979.2021.1944026

135. Sun Q, Hu S, Lou Z, Gao J. The macrophage polarization in inflammatory dermatosis and its potential drug candidates. *Biomedicine Pharmacotherapy*. (2023) 161:114469. doi: 10.1016/j.biopha.2023.114469

136. Bratovcic A. Antioxidant enzymes and their role in preventing cell damage. *Act Scie Nutr*. (2020) 4:01–7. doi: 10.31080/ASNH.2020.04.0659

137. Halliwell B, Gutteridge JMC. *Free Radicals in Biology and Medicine*. Oxford, United Kingdom: Oxford University Press (2015). doi: 10.1093/acprof:oso/9780198717478.001.0001

138. Sies H. Hydrogen peroxide as a central redox signaling molecule in physiological oxidative stress: Oxidative eustress. *Redox Biol*. (2017) 11:613–9. doi: 10.1016/j.redox.2016.12.035

139. Guo C, Ning X, Zhang J, Zhang C, Wang J, Su L, et al. Ultraviolet B radiation induces oxidative stress and apoptosis in human lens epithelium cells by activating NF-κB signaling to down-regulate sodium vitamin C transporter 2 (SVCT2) expression. *Cell Cycle*. (2023) 22:1450–62. doi: 10.1080/15384101.2023.2215084

140. McGlone CL, Christian L, Schmeusser B, Liu L, Chalfant CE, Stephensen DJ, et al. Evidence for systemic reactive oxygen species in UVB-mediated microvesicle formation. *Photochem Photobiol*. (2022) 98:242–7. doi: 10.1111/php.13494

141. de Jager TL, Cockrell AE, Du Plessis SS. Ultraviolet light induced generation of reactive oxygen species. *Adv Exp Med Biol*. (2017) 996:15–23. doi: 10.1007/978-3-319-56017-5_2

142. Sitaula S, Burris TP. Cholesterol and other steroids. In: *Encyclopedia of Cell Biology*. Amsterdam, Netherlands: Elsevier (2016). p. 173–9. doi: 10.1016/B978-0-12-394447-4.10021-5

143. Sun Y, Wang J, Long T, Qi X, Donnelly L, Elghobashi-Meinhardt N, et al. Molecular basis of cholesterol efflux via ABCG subfamily transporters. *Proc Natl Acad Sci U.S.A*. (2021) 118:e2110483118. doi: 10.1073/pnas.2110483118

144. Sherwood ER, Burelbach KR, McBride MA, Stothers CL, Owen AM, Hernandez A, et al. Innate immune memory and the host response to infection. *J Immunol*. (2022) 208:785–92. doi: 10.4049/jimmunol.2101058

145. Saeed S, Quintin J, Kerstens HHD, Rao NA, Aghajanirefah A, Matarese F, et al. Epigenetic programming of monocyte-to-macrophage differentiation and trained innate immunity. *Science*. (2014) 345:1251086. doi: 10.1126/science.1251086

146. Drummer C, Saaoud F, Shao (邵颖) Y, Sun (孙宇) Y, Xu (徐克曼) K, Lu (路一凡) Y, et al. Trained immunity and reactivity of macrophages and endothelial cells. *Arterioscler Thromb Vasc Biol*. (2021) 41:1032–46. doi: 10.1161/ATVBAHA.120.315452

147. Rauchbach E, Zeigerman H, Abu-Halaka D, Tirosh O. Cholesterol induces oxidative stress, mitochondrial damage and death in hepatic stellate cells to mitigate liver fibrosis in mice model of NASH. *Antioxidants (Basel)*. (2022) 11:536. doi: 10.3390/antiox11030536

148. Bekkering S, Arts RJW, Novakovic B, Kourtzelis I, van der Heijden CDCC, Li Y, et al. Metabolic induction of trained immunity through the mevalonate pathway. *Cell*. (2018) 172:135–46.e9. doi: 10.1016/j.cell.2017.11.025

149. Netea MG, Joosten LAB, Latz E, Mills KHG, Natoli G, Stunnenberg HG, et al. Trained immunity: A program of innate immune memory in health and disease. *Science*. (2016) 352:aaf1098. doi: 10.1126/science.aaf1098

150. Cheng S-C, Quintin J, Cramer RA, Shepardson KM, Saeed S, Kumar V, et al. mTOR- and HIF-1α-mediated aerobic glycolysis as metabolic basis for trained immunity. *Science*. (2014) 345:1250684. doi: 10.1126/science.1250684

151. Tall AR, Yvan-Charvet L. Cholesterol, inflammation and innate immunity. *Nat Rev Immunol*. (2015) 15:104–16. doi: 10.1038/nri3793

152. Pike LJ. Rafts defined: a report on the Keystone Symposium on Lipid Rafts and Cell Function. *J Lipid Res*. (2006) 47:1597–8. doi: 10.1194/jlr.E600002-JLR200

153. Peng J, Luo F, Ruan G, Peng R, Li X. Hypertriglyceridemia and atherosclerosis. *Lipids Health Dis*. (2017) 16:233. doi: 10.1186/s12944-017-0625-0

154. Benghalem I, Meziane W, Hadjidj Z, Ysmail-Dahlouk L, Belamri A, Mouhadjer K, et al. High-density lipoprotein immunomodulates the functional activities of macrophage and cytokines produced during ex vivo macrophage-CD4 + T cell crosstalk at the recent-onset human type 1 diabetes. *Cytokine*. (2017) 96:59–70. doi: 10.1016/j.cyto.2017.03.001

155. Goicoechea L, Conde de la Rosa L, Torres S, García-Ruiz C, Fernández-Checa JC. Mitochondrial cholesterol: Metabolism and impact on redox biology and disease. *Redox Biol*. (2023) 61:102643. doi: 10.1016/j.redox.2023.102643

156. Zhang Q, Wang J, Yadav DK, Bai X, Liang T. Glucose metabolism: the metabolic signature of tumor associated macrophage. *Front Immunol*. (2021) 12:702580. doi: 10.3389/fimmu.2021.702580

157. Curi R, De Siqueira Mendes R, De Campos Crispin LA, Norata GD, Sampaio SC, Newsholme P. A past and present overview of macrophage metabolism and functional outcomes. *Clin Sci*. (2017) 131:1329–42. doi: 10.1042/CS20170220

158. Newsholme P, Curi R, Gordon S, Newsholme EA. Metabolism of glucose, glutamine, long-chain fatty acids and ketone bodies by murine macrophages. *Biochem J*. (1986) 239:121–5. doi: 10.1042/bj2390121

159. Newsholme P, Gordon S, Newsholme EA. Rates of utilization and fates of glucose, glutamine, pyruvate, fatty acids and ketone bodies by mouse macrophages. *Biochem J*. (1987) 242:631–6. doi: 10.1042/bj2420631

160. Desai BN, Leitinger N. Purinergic and calcium signaling in macrophage function and plasticity. *Front Immunol*. (2014) 5:580. doi: 10.3389/fimmu.2014.00580

161. Nunes P, Demaurex N. The role of calcium signaling in phagocytosis. *J Leukocyte Biol*. (2010) 88:57–68. doi: 10.1189/jlb.0110028

162. Forman HJ, Torres M. Reactive oxygen species and cell signaling: respiratory burst in macrophage signaling. *Am J Respir Crit Care Med*. (2002) 166:S4–8. doi: 10.1164/rccm.2206007

163. Clapham DE. Calcium signaling. *Cell*. (2007) 131:1047–58. doi: 10.1016/j.cell.2007.11.028

164. Görlach A, Bertram K, Hudecova S, Krizanova O. Calcium and ROS: A mutual interplay. *Redox Biol*. (2015) 6:260–71. doi: 10.1016/j.redox.2015.08.010

165. Malli R, Graier WF. Mitochondrial Ca2+ channels: Great unknowns with important functions. *FEBS Lett*. (2010) 584:1942–7. doi: 10.1016/j.febslet.2010.01.010

166. Bertero E, Maack C. Calcium signaling and reactive oxygen species in mitochondria. *Circ Res*. (2018) 122:1460–78. doi: 10.1161/CIRCRESAHA.118.310082

167. Yoshida A, Yoshino F, Makita T, Maehata Y, Higashi K, Miyamoto C, et al. Reactive oxygen species production in mitochondria of human gingival fibroblast induced by blue light irradiation. *J Photochem Photobiol B*. (2013) 129:1–5. doi: 10.1016/j.jphotobiol.2013.09.003

168. Golovynska I, Golovynskyi S, Qu J. Comparing the impact of NIR, visible and UV light on ROS upregulation via photoacceptors of mitochondrial complexes in normal, immune and cancer cells. *Photochem Photobiol*. (2023) 99:106–19. doi: 10.1111/php.13661

169. Sommer AP. Mitochondrial cytochrome c oxidase is not the primary acceptor for near infrared light-it is mitochondrial bound water: the principles of low-level light therapy. *Ann Transl Med*. (2019) 7:S13. doi: 10.21037/atm.2019.01.43

170. Cheng G, Zielonka M, Dranka B, Kumar SN, Myers CR, Bennett B, et al. Detection of mitochondria-generated reactive oxygen species in cells using multiple probes and methods: Potentials, pitfalls, and the future. *J Biol Chem*. (2018) 293:10363–80. doi: 10.1074/jbc.RA118.003044

171. Eisberg RM, Resnick R. *Quantum physics of atoms, molecules, solids, nuclei, and particles. 2nd ed*. New York: Wiley (1985). 1 p.

172. Griffiths DJ, Schroeter DF. Introduction to quantum mechanics. *Third edition*. Cambridge ; New York, NY: Cambridge University Press (2018). 495 p.

173. Rennie R ed. *A dictionary of chemistry. Seventh edition*. Oxford: Oxford University Press (2016). 594 p.

174. Wisniak J. John william draper. *Educación Química*. (2013) 24:215–23. doi: 10.1016/S0187-893X(13)72465-0

175. Menzel JP, Noble BB, Blinco JP, Barner-Kowollik C. Predicting wavelength-dependent photochemical reactivity and selectivity. *Nat Commun*. (2021) 12:1691. doi: 10.1038/s41467-021-21797-x

176. Moore C, Cevikbas F, Pasolli HA, Chen Y, Kong W, Kempkes C, et al. UVB radiation generates sunburn pain and affects skin by activating epidermal TRPV4 ion channels and triggering endothelin-1 signaling. *Proc Natl Acad Sci U S A*. (2013) 110:E3225–3234. doi: 10.1073/pnas.1312933110

177. Zhang M, Ma Y, Ye X, Zhang N, Pan L, Wang B. TRP (transient receptor potential) ion channel family: structures, biological functions and therapeutic interventions for diseases. *Signal Transduct Target Ther*. (2023) 8:261. doi: 10.1038/s41392-023-01464-x

178. Wicks NL, Chan JW, Najera JA, Ciriello JM, Oancea E. UVA phototransduction drives early melanin synthesis in human melanocytes. *Curr Biol*. (2011) 21:1906–11. doi: 10.1016/j.cub.2011.09.047

179. Fiedorczuk K, Letts JA, Degliesposti G, Kaszuba K, Skehel M, Sazanov LA. Atomic structure of the entire mammalian mitochondrial complex I. *Nature*. (2016) 538:406–10. doi: 10.1038/nature19794

180. Carbone L. Pain in laboratory animals: the ethical and regulatory imperatives. *PLoS One*. (2011) 6:e21578. doi: 10.1371/journal.pone.0021578